TOWARDS A UNIFIED UNDERSTANDING OF EUKARYOTIC CELL MOTILITY

By

Jonathan Scott Gruver

Dissertation

Submitted to the Faculty of the

Graduate School of Vanderbilt University

in partial fulfillment of the requirements

for the degree of

DOCTOR OF PHILOSOPHY

In

Pharmacology

May 2010

Approved:

Chang Y. Chung

H. Alex Brown

Todd Graham

Roger Colbran

Brian Wadzinski

TABLE OF CONTENTS

DEDICATION

This work is dedicated to three important people. My parents Larry and Phyllis Gruver have taken what can only be described as a patient approach to my development and all of my bets qualities I learned from them. My debt to them is immense and I anxiously await the day that I can begin to give back to them in a serious way. Finally, I also dedicate this work to my wife, Xiufeng Song. She, more than anyone, listened to my boasts and whines and always understood when I needed a little more time during this rollercoaster ride that is called Graduate School.

ACKNOWLEDGEMENTS

They say that it takes a village to raise a child and here at this village called Vanderbilt University I have received unbelievably generous support from a large number of its inhabitants. Of course, I must begin by thanking my mentor, Dr. Chang Chung, whose patience gave me room to grow as a scientist and who was always supportive. It was Chang, for example, who introduced me to Dr. Phil Crooke and also to my coauthor Alka Potdar. Their acquaintance greatly enriched my graduate experience. I am also thankful for a training grant from the Department of Pharmacology and to the NIH for funding my work. The member of the Chung lab, past and present, have always provided an enjoyable atmosphere so that the sometimes tedious work seldom felt tedious. I also thank my committee members, Dr. Alex Brown (chair), Dr. Roger Colbran, Dr. Todd Graham, and Dr. Brian Wadzinski for their encouragement and honest, yet helpful, criticisms. Early in my tenure here I met Dr. John Wikswo of the Department of Biomedical Engineering who introduced me to the wonders of microfabrication. Also in those earliest times, I was fortunate to have met Dr. Phil Crooke of the Department of Mathematics. My lack of formal in mathematics left me a little insecure as I explored the field of mathematical modeling of biological systems and Phil's encouragement provided the confidence that I needed. I would like to thank my coauthors, especially Alka Potdar, for excellent collaboration. I received many awards to cover travel expenses so that I could present my work including the annual Student Travel Award

from the Graduate School, a travel award from the Graduate Student Council, a travel award from the Department of Pharmacology, a travel fellowship from the Japanese Society for the Promotion of Science, and an Oberwolfach Fellow travel award from the National Science Foundation. I thank Dr. Emmanuelle DiBennedetto of the Department of Mathematics for the invitation to Oberwolfach, Germany to participate in the workshop on Mathematical Biology. Finally, I would again like to thank Drs. Chung, Brown, and DiBennedetto for writing letters of recommendation and for their assistance in obtaining a postdoctorall position.

LIST OF FIGURES

Figure Page

LIST OF TABLES

Table Page

CHAPTER I

INTRODUCTION TO CELL MOTILITY AND *DICTYOSTELIUM DISCOIDIES*

Cell motility in physiology and pathology.

Cell motility plays critical roles in many biological processes [1, 2]. Amidst the earliest stages of the development of the vertebrate embryo, a small group of cells migrates in between the still forming endoderm and ectoderm. These cells form the mesoderm and eventually give rise to the musculature, circulatory system, and skeleton. Cell motility also is fundamentally involved in wound healing. For example, when a vertebrate suffers an injury, motile cells migrate into the injury site, eliminate infection, lay down extracellular matrix, lead to revascularization, and eventually close the wound. Unfortunately, cell motility is also an important step in the deadly metastasis of primary tumors, where malignant cells leave the original tumor and migrate into other hospitable tissues to form secondary, and often lethal, tumors. Considering these examples, it is not a stretch to say that cell motility is intimately involved in the beginning, plays key roles in maintaining, and, all too often, leads to the end of a multicellular organism.

Types of cell motility.

During physiological and pathological processes, cell motility is guided, or *directed*, by external cues. Various cues are recognized by different cell types in different contexts, including soluble chemicals, matrix-bound chemicals, electrical/magnetic fields, and spatial variability in the local mechanical properties of tissues [3]. Perhaps the best understood form of directed motility is chemotaxis, or directed motility in the presence of a soluble gradient of ligand. In many examples, a particular ligand produced and secreted by a cell or tissue serves to attract chemotactic cells. This ligand is therefore referred to as a chemoattractant. In other cases, such as in axon guidance, secreted substances serve to repel chemotactic cells. These substances are defined as chemorepellents. During chemotaxis, and indeed all forms of directed cell motility, the movements of the cell are guided or biased by external information.

When chemotactic cells are experimentally placed in simple environments lacking any spatial variability, they undergo a spontaneous form of motility often called *random motility*. However, as shown in Fig. 1, the path of a cell during such motility is not, in a quantitative sense, truly random. Instead, the directions of successive movements are correlated for some length of time in between reorientations. To reflect this fact we will refer to such motility as *non-directed motility*. It is important to note that, in contrast to directed motility, non-directed motility occurs strictly as the result of intrinsically driven subcellular processes.

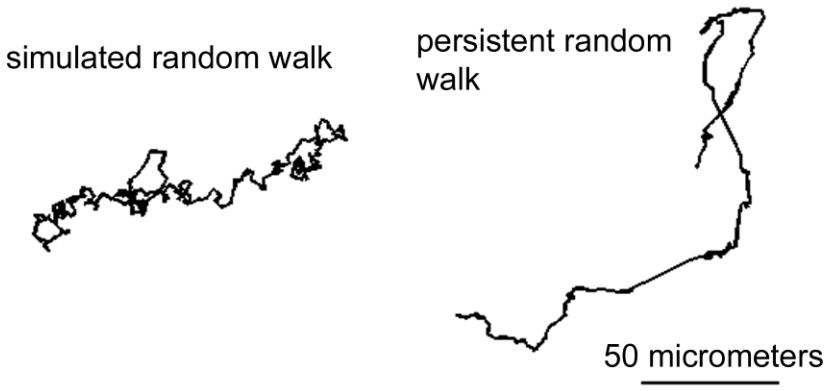

Figure 1 **A comparison of a simulation of a simple random walk (left) with data from a *wt Dictyostelium* cell undergoing non-directed or "random motility" (right).** The data from the cell is an example of a persistent random walk, where the direction between successive movements are correlated. To allow for proper comparison, it should be noted that the mean and standard deviation of the step size for simulation is identical to that of the cell path.

Cell polarity, where a cell is elongated about an axis, is a common feature of both forms of motility. Experimentally, however, the two forms of motility are often studied independently and from different points of view. This perhaps reflects a belief that the cell polarity seen in directed and non-directed are different in origin. In the study of non-directed motility, it is common to attempt to isolate the components responsible for the spontaneous formation of polarity (see for example [4]). Therefore, the focus tends to be on cytoskeletal proteins, such as F-actin and myosin II, and their modifiers. In contrast, during directed motility polarity is thought to be driven by externally generated signals, and therefore, is typically approached from the perspective of signal transduction [5]. The goal, then, in most studies of chemotaxis is to identify the signaling pathways that translate the externally generated signals into polarity and directed movement. Clearly, directed motility is cell motility with a *purpose*, allowing for

pattern formation during development and specific responses to injuries. Furthermore, it is not evident that in the complex multicellular environment, motile cells ever experience an environment without some spatial signal capable of influencing their motility. Nonetheless, in this dissertation, I argue that critical insights into mechanisms of directed cell motility can be gained by the study non-directed motility.

***Dictyostelium discoideum*: a model system for the study of eukaryotic cell motility.**

Dictyostelium discoideum is a nominally single-celled eukaryotic organism that lives on the floor of temperate forest where they feed on bacteria and single-celled fungi. When cultured in the presence of food, the cells are referred to as *vegetative.* In the vegetative state, they are capable of non-directed motility and also utilize their ability to sense folic acid (here a bacterially-derived metabolic by-product) to undergo chemotaxis in an effort to find and engulf bacteria. When deprived of nutrient sources, *Dictyostelium* initiates a truly remarkable reproductive strategy-approximately 10^7 individuals begin to communicate via the synchronized, pulsatile release of cAMP, differentiate, and develop into a multicellular, reproductive structure (Fig.2). In *Dictyostelium*, cAMP acts as a first messenger, serving as a chemoattractant cue to draw surrounding cells to central location, forming a loose aggregate. Cells that have been starved and are sensitive to cAMP are called *developed*. During development cells begin to differentiate into a small number of cell types which eventually develop to form a multicellular fruiting body, complete with stalk and spores (Fig. 2B).

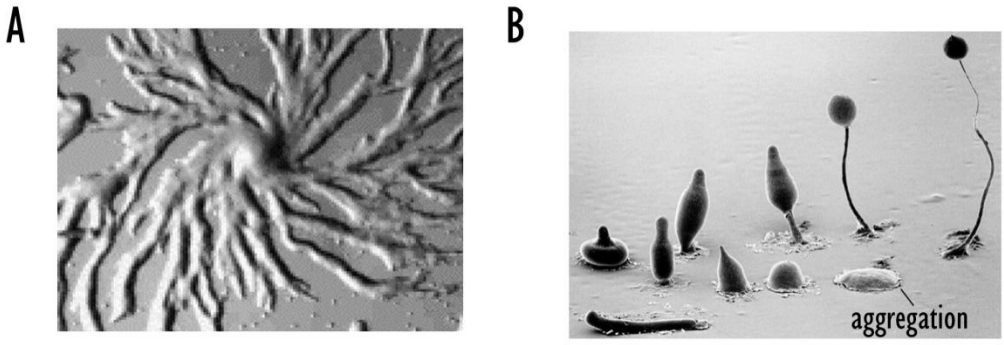

Figure 2 The **late stages of the *Dictyostelium* developmental cycle.** A) Streams of thousands of cells form during aggregation towards a developmental center (located in the middle of the of the image). The initial stages of cell differentiation begin during streaming. The result of aggregation is the formation of the loose mound shown in the lower left of (B). From the loose mound, a stalk is formed and elongates while the remaining cells migrate up the stalk and differentiate into spores. Images from http://dictybase.org/Multimedia/index.html.

Many pathways and processes present in human cells are also conserved in *Dictyostelium. Dictyostelium* is commonly used as a simple model system for the study of pattern formation during multicellular development, cytoskeletal regulation, signal transduction, and cell motility [6]. The availability of recombinant genetics allows for easy deletion of genes and expression of GFP fusion proteins for *in vivo* analysis of molecular processes. The genome of 34 Mbs has been fully sequenced, revealing the presence of ~12,500 protein-coding genes on 6 chromosomes [7]. A stringent test for the presence of 287 human disease genes revealed that *Dictyostelium* possessed 64, confirming its utility as a model system for medical related cell and developmental processes.

Dictyostelium cells are ~10-20 μm long when polarized. The speed of *Dictyostelium* motility depends on the type of motility (chemotactic vs. non-directed)

and the developmental stage. For example, the mean speed of a vegetative cell undergoing non-directed motility would be around 3-6 μms/minute while a developed cell undergoing chemotaxis might reach mean speeds as high as 20 μms/minute. This is slightly faster than the mean speed of neutrophils and considerably faster than most other motile human cells. The rapidity of the movement allows for short assay times and the acquisition of larger datasets.

Cell polarity and gradient sensing.

> *"The morphologists is accustomed to speak of a "polarity" of the cell, meaning thereby a symmetry of visible structure about a particular axis…The* ***morphological*** *polarity is accompanied by, and is but the outward expression (or part of it) of a true* ***dynamical*** *polarity, or distribution of forces"* [8].

The importance of being polarized.

The concept of polarity is long thought to be crucial for cell motility [9]. Unfortunately, the term polarity is often used loosely to describe two related phenomena. First, polarity often refers to a polarity inherent in the shape of the cell. We will refer to this form of polarity and *morphological* polarity as defined in the opening quote [8]. Morphological polarity is readily visible under the light microscope, where the cell is described as having a leading edge, a broad zone at one pole of the cell in the direction the cell is currently traveling, and a relatively narrow trailing edge or uropod (Fig. 3). *Dynamical* polarity, on the other hand, refers to an asymmetric distribution of sub-cellular structure or components, including signaling molecules and cytoskeletal

proteins. Dynamical polarity can be visualized by the imaging of GFP labeled molecules or of traction forces applied by the cell to the substratum via traction force microscopy (Fig. 3B) [10]. Clearly, these two concepts are related as dynamical polarity ultimately gives rise to morphological polarity. However, distinction between these two concepts is important as it is possible to study dynamical polarity in a cell that, as a result of Latrunculin treatment, lacks morphological polarity (Fig. 3C) [11]. Similarly, in brightfield imaging experiments, it is possible to examine morphological polarity without any knowledge of the underlying structural polarity.

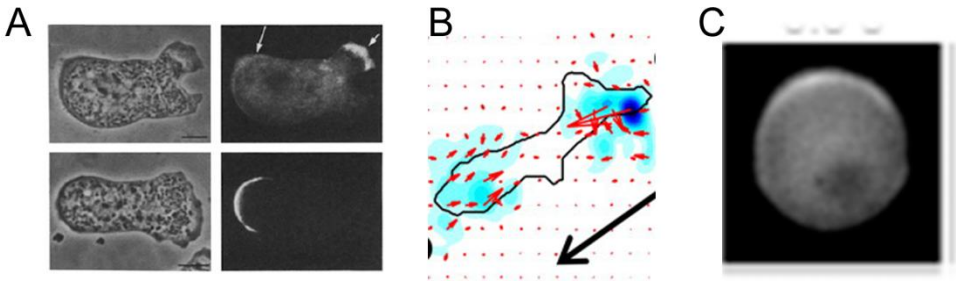

Figure 3 **Cell polarity in it's various guises.** A) Side by side images of morphological polarity (left, brightfield images) and immunofluorescent staining of F-actin (top) and myosin II (bottom). Cells are polarized with the uropod to the left and the leading edge on the right. Arrows in the top left image point to F-actin enrichment at the leading edge and, to a lesser extent, the uropod [12]. B) Example of dynamical polarity as evidenced by traction force microscopy. Cell is outlined in black and the arrow indicates the direction traveling. The red arrows indicate the magnitude and direction of traction forces [10]. C) A cell expressing the PH domain of Crac fused to GFP is treated with Latrunculin A and stimulated with a gradient of chemoattractant. The latrunculin eliminates morphological polarity, yet the PH domain localizes to the membrane in a polarized fashion, indicating the presence dynamical polarity [13].

The concept of cell polarity is important for cell motility in that efficient motility requires spatial segregation of subcellular processes. At the mechanical level, the segregation of F-actin polymerization to the front, and to a lesser extent, the rear, provides the force required for protrusion of the leading edge membrane and assists in myosin II-mediated contraction of the uropod, respectively (Fig. 3A). The processes of actin polymerization at the leading edge and F-actin/myosin II contraction at the uropod is often described as a mechanical cycle [14], producing movement similar to the movements of an inch worm. However, the cycle is not known to possess any regularity [15], resulting in complex patterns of cell displacement.

Signal transduction and cell polarity.

The sensitivity of chemotactic cells to weak concentration gradients has led to a focus on the signal transduction pathways that sense the gradients and appropriately bias motility. The basic components of the gradient sensing signal transduction pathway are shown in Fig. 4 and will be momentarily discussed in greater. A powerful concept in studying these signal transduction pathways has been *gradient amplification*. Gradient amplification refers to a cells ability to convert shallow, noisy chemoattractant concentration gradients into stronger internal signaling gradients. Gradient amplification has been demonstrated in *Dictyostelium* [11, 16] and neutrophils [17].

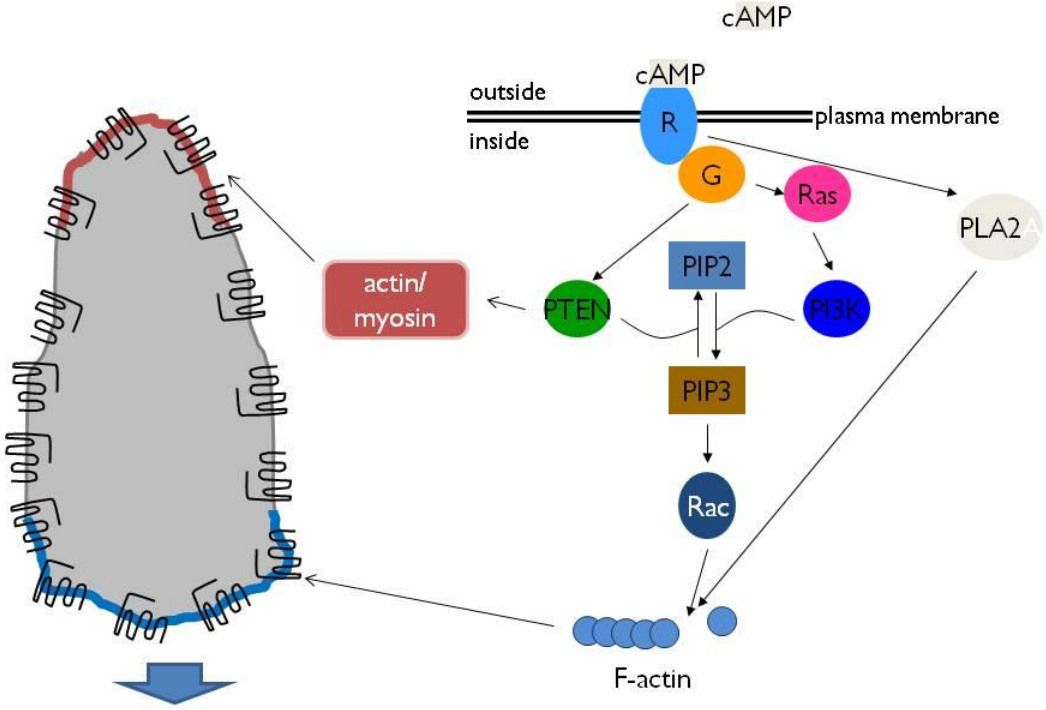

Figure 4 **Some of the signal transduction pathways implicated in chemoattractant signaling.** The chemoattractant receptor, cAR1, is uniformly distributed throughout the membrane. cAR1 is differentially occupied by chemoattractant across the cell body and therefore results in spatial segregation F-actin-based protrusion at the leading edge of the cell (the arrow indicates the direction of travel) and F-actin/myosin II based retraction at the uropod.

Subcellular components and their localization.

> *"But in all probability, the dynamical polarity or asymmetry of the cell is a very complicated phenomenon: for the obvious reason that, in any system, one asymmetry will tend to beget another."* [8]

In this section we will review the localization of key components involved in chemotaxis. Due to evolutionary conservation, many pathways identified in *Dictyostelium* are shared in mouse and human chemotactic cells.

The process of chemotaxis begins with gradient sensing and gradient sensing begins with the binding of the chemoattractant, cAMP, to the chemoattractant receptor. It was proposed that the receptor might accumulate at the leading edge in order to simplify gradient sensing. In *Dictyostelium* cAR1 is a G protein coupled receptor and it localization has been examined by labeling the receptor with GFP and live-cell imaging. The receptor appears to be uniformly distributed in the membrane as shown in Figure 5. The uniform distribution allows for greater sensitivity to multiple, competing chemoattractant sources [18]. Therefore, a cell remains open to detecting new ligand sources rather than prematurely locking on one direction.

The diffusion of the receptor within the membrane could have significant consequences for the sensing of chemoattractant gradients. Diffusion is typically thought of as a smoothing process, where a locally high concentration of one substance eventually becomes uniformly distributed. During chemotaxis, higher receptor occupancy within one region of the cell drives the directionality of the motility. Thus, the diffusion of the receptor would serve to reduce the perceived strength of the gradient as the higher density of occupied receptors in the leading region of the cell would diffuse outward. For this reason, the diffusion of the receptor has been studied in some detail. Originally, the diffusion of the receptor was measured by tracking the

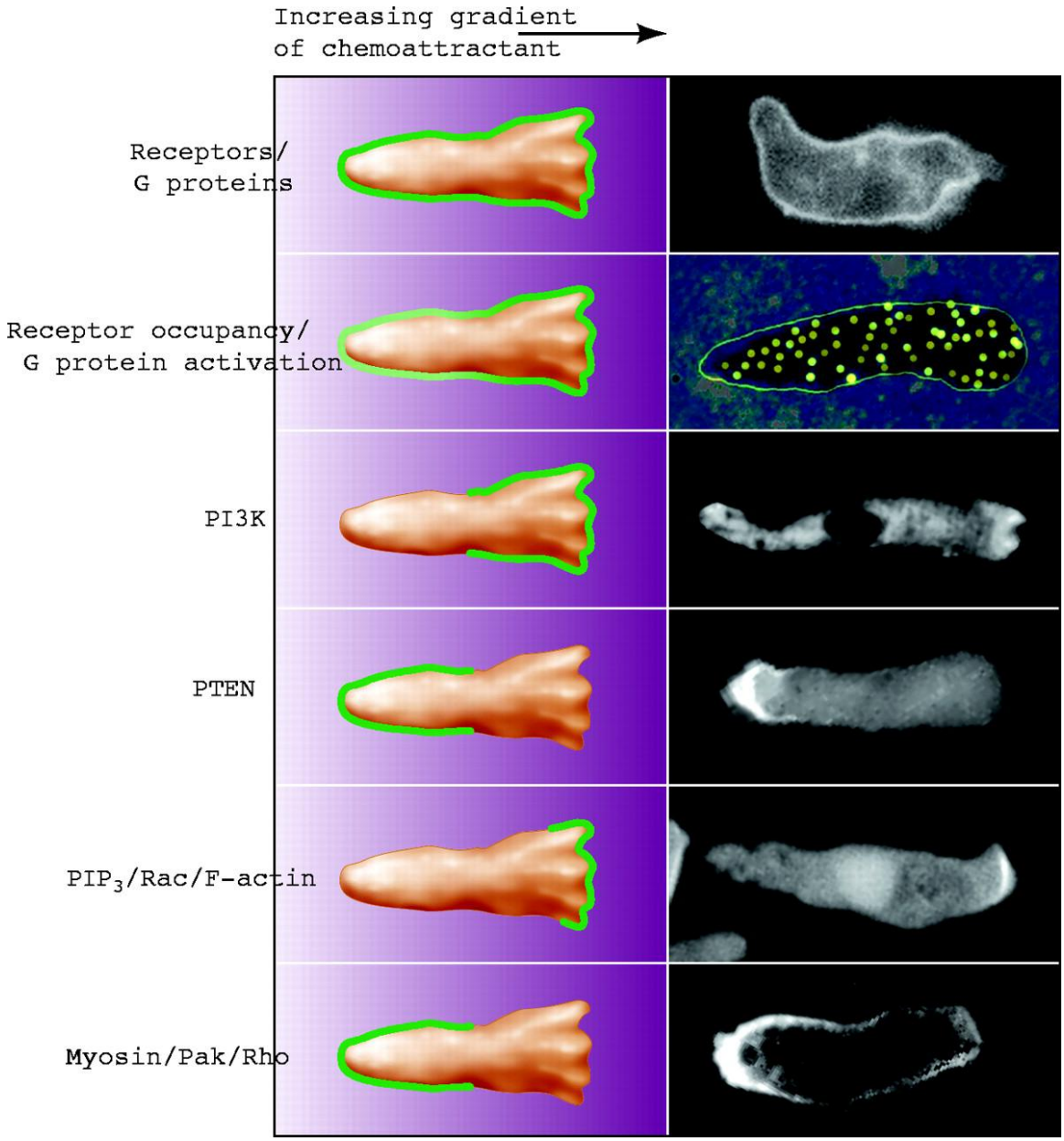

Figure 5 **The polarized localization of signaling pathways regulating cell polarity and chemotaxis in *Dictyostelium*.** Left column contains schematic representations of fluorescent micrographs in right column. Figure from [19].

motility of single molecules of fluorescently labeled cAMP bound to the chemoattractant receptor. The receptor was found to diffuse laterally within the membrane with a diffusion coefficient of D=2.7+/-1.1 x 10^{-10} cm^2/second [20].

Later, the diffusion of YFP-labeled cAR1 was studied in living cells [21]. In this study, the diffusion of the receptor was shown to be more complicated, suggesting two populations of receptors, one diffusing and one immobile. The diffusion coefficient of the mobile population was found to be D=1.7 x 10^{-9} cm^2/second. Interestingly, the fraction of mobile and immobile receptors depended upon the polarity of the cell with a higher proportion of mobile receptors in the anterior of chemotaxing cells. Repeating the experiments in cells lacking the α_2-subunit of the heterotrimeric G-protein in *Dictyostelium*, the anterior and posterior of the cell possessed the same proportion of mobile and immobile receptors, suggesting that interaction between receptor and G-proteins to be a major contributor to receptor immobilization.

The localization of downstream signaling molecules has also been studied in detail. The heterotrimeric-G-protein $\beta\gamma$ subunits were fluorescently labeled and imaged during chemotaxis [22]. Their localization was predominately uniform with a slight accumulation at the leading edge. Attempts have also been made to image the spatial activation of the G-protein via FRET with the anticipation that there should be higher activation in the leading edge than the posterior [16, 23]. The difference in receptor occupancy from anterior to posterior, as measured in these studies, is very weak. The

spatial resolution of these studies appears to be hampered by the weak FRET signal and proper measurement awaits improved experimental methods.

The next step in the pathway, downstream from the $\beta\gamma$ subunit of the heterotrimeric G-protein is thought to be Ras (Fig. 4) [24]. *Dictyostelium* possess 18 isoforms of Ras, making the identification of specific genes difficult, yet through a combination of multiple gene deletions and the expression of a dominant negative mutant, Ras has been shown to play a key role in the transmitting the signal from the G-protein to pathways further downstream. RasG is uniformly distributed, yet the expression of a GFP-labeled activated Ras binding domain, revealed activated Ras to localize to the leading edge of the cell and sites of protrusion.

Downstream from Ras, the PI3K pathway also appears to be important for gradient sensing [25]. PI3K catalyzes the addition of a phosphate group to PI(4,5)P2 at the 3' position on the inositol ring to form PI(3,4,5)P3 (PIP3) (Fig. 4 and 5). Similarly to activated Ras, all isoforms localize to the leading edge and membrane protrusions during chemotaxis. Constitutive membrane targeting via fusion with a myristoylation sequence results in multiple protrusions and poor coordination of movement. *Dictyostelium* has 6 type I PI3Ks, all of which have been genetically deleted either singly or in combination. Cells lacking either two or three type I PI3Ks were claimed to be deficient in sensing shallow gradients and accordingly, chemotax poorly [25, 26].

The enzyme PTEN performs the counters the reaction to PI3K, converting PIP3 to PI(4,5)P2. Genetic deletion of PTEN resulted in a broad, poorly defined leading edge and

multiple sites of membrane protrusion [25, 27]. The poor cytoskeletal organization is reflected in reduced accuracy and speed during chemotaxis. Sharply contrasting with the localization of PI3K, PTEN-GFP localizes to the cell membrane in the lateral and rear regions (Fig. 5). The near mutual exclusion of the localization of PI3K and PTEN leads to a strong intracellular gradient of PIP3 (Fig. 5).

PIP3, as the enzymatic product of PI3K, is rapidly generated in response to chemoattractant stimulation [25]. Many proteins with different domains bind to and are activated by PIP3, most notably pleckstrin-homology domain (PH) containing proteins such as protein kinase B (PKB), also known as Akt. During chemotaxis, the dynamics of PIP3 can be visualized in the cell via the expression of a PH domain fused to GFP. The localization of the PH domain of Akt is dynamic and closely follows the localization of PI3K. Typically, it is at the level of PIP3 dyanamics, whereby simultaneously measuring the steepness of the chemoattractant concentration gradient and the steepness of the PIP3 gradient as evidenced by a 3'-phosphoinositde specific PH domain, that gradient amplification is examined.

The notion that the PI3K/PTEN pathway was a key regulator of cell polarity in *Dictyostelium* was attractive in its simplicity and led to numerous studies where it was revealed that PI3K/PTEN regulated cell polarity in a number of diverse systems [28-33]. However, work by the Kay lab called into question the necessity of PI3K signaling in *Dictyostelium* by genetically deleted all type I PI3Ks in the same cell [34]. Although these pentuple knockout cells were shown to be somewhat defective in chemotaxis, it was clear that they were able to sense chemoattractant gradients and polarize accordingly.

This finding resulted in the idea that PI3K played an important, yet somewhat redundant role in chemoattractant sensing and cell polarity. A role for phospholipase A_2 was discovered by a genetic screen designed to isolate mutations that, when combined with PI3K inhibition, would lead to chemotactic defects (Fig. 4) [35]. PI3K activity was shown to be independent of PLA_2, yet PLA_2 activity was required for chemotaxis in the absence of PI3K. *Dictyostelium* PLA_2 was shown to be capable of using phosphatidylcholine as a substrate and also to be inhibited by free $Ca^{2+.}$ Importantly, GFP-labeled PLA_2 is cytosolic in localization nor did it show any appreciable polarity in its subcellular localization during chemotaxis.

Another pathway that has been shown to act in parallel with PI3K in *Dictyostelium* is the TOR2 pathway [36]. The TOR2 kinase complex is known to phosphorylate the hydrophobic loop of PKB and protein kinase C (PKC). In *Dictyostelium*, the TOR2 complex was shown to phosphorylate both isoforms of PKB, PKBA and PKBR. PKBA contains a PH-domain and is activated by both PIP3 amd TPR2. The second isoform, PKBR, does not contain a PH domain yet is myristoylated, and therefore constitutively localized to the plasma membrane and activated via TOR2 in a PIP3-indepedent manner.

The polarity of the F-actin/myosin cytoskeleton during motility has been appreciated for longer than polarized distributions of signaling molecules [12]. In a cell with morphological polarity, F-actin production is predominantly at the leading edge, where it is thought to provide the protrusive force required for the extension of pseudopodia or lamellapodia. To a lesser extent, F-actin also accumulates in the uropod

where it provides a scaffold for the assembly of myosin II filaments. Myosin II localizes exclusively to the uropod where in conjunction with F-actin, it generates the force necessary for the retraction of the uropod.

Experimentally established chemoattractant ranges for chemotaxis.

Dictyostelium and chemotactic cells, in general, are exquisitely sensitive to weak and noisy concentration gradients. In 1989, Fisher *et al.* measured the accuracy of chemotaxis in a custom chemotaxis chamber [37]. The chamber allowed for the generation of linear concentration profiles with defined ranges and midpoints. A linear concentration profile can be completely described by two measurements, the midpoint, and ∇c, the change in concentration, Δc over distance, Δx. First the varied the midpoint and ∇c simultaneously and found a threshold for detectable chemotaxis at a midpoint of 25 pM with ∇c =25 nM/ μm.

Song *et al.* used microfluidic devices to generate linear gradients and found the threshold to be ∇c = 0.0033 nM/ μm, three orders of magnitude lower [15]. van Haastert and Postma also tested cells for the lowest value of ∇c capable of producing directed movement [38]. Their result of ∇c = 0.005 nM/ μm, very close to Song *et al.* The reason for the discrepancy between Fisher and the more recent experiments is not clear, but all three measurements highlight the sensitivity of cell to weak gradients. This can be appreciated by considering that 1 nM ~0.6 molecules/ μm^3, suggesting that at these low concentrations, cells are counting in the range of 100-1000 molecules at any one time. It is well appreciated that at concentrations this low, noise due to thermal

fluctuations in ligand concentration can seriously affect the cells ability to sense concentration gradients.

Theoretical understanding of gradient sensitivity.

Given the exquisite sensitivity of chemotactic cells, many researchers have attempted to arrive at a theoretical understanding of the ability of cells to sense small differences across the cell body. All the models presented here assume that the receptor is evenly distributed within the cell membrane and that the cell membrane is evenly distributed within the chemoattractant gradient. Although the receptor does appear to be evenly distributed within membrane (Fig.), given the dynamic morphology of the chemotaxing cell it is not clear how valid the second assumption is. Another caveat of many of these approaches that must be appreciated is that many of them depend upon estimates of the equilibrium dissociation constant, K_d, for the chemoattractant receptor and the chemoattractant. The value of this constant varies considerably in the literature, presumably due to multiple affinity states and experimental variation [39].

A simple model for receptor occupancy was given in [15], where it was shown that, assuming that binding takes place at chemical equilibrium, fractional receptor occupancy, θ, can be estimated from

$$\theta = \frac{c}{c + K_d},$$

where c is the chemoattractant concentration and K_d is the familiar equilibrium dissociation constant. Using this relationship to compare the receptor occupancy in the front and rear of the cell, it can be estimated that, at the low threshold for directed movement of ∇c = 0.033 nM/ μm, there are 128 receptors occupied at the front half and 120 occupied in the rear half of a cell in the middle of the gradient. This implies when measuring differences across the cell body, cells are *extremely* sensitive single molecule counters. This calculation was made using a value for K_d =100 nM. Clearly, using one of the lower range experimentally determined values of K_d would lead to larger differences in receptor occupancy between the front and back of the cell.

Although the difference in receptor occupancy over the cell body is an important quantity, it is also important to know the average receptor occupancy of the cell. This is due to the fact that receptor-ligand interactions are a stochastic process. This type of stochastic process, where each binding event is statistically independent, is known as a Poisson process, and has a simple relationship between the mean number of occupied receptors, N, and the average fluctuation about that mean. Under these conditions, the typical fluctuation about N is given by $\sqrt{N}$ [40, 41]. Revisiting the threshold experiments of Song et al, a total of 248 receptors would be occupied, giving $\sqrt{N} \cong 15$. Similar conclusions are found from van Haastert and Postma. Thus the typical fluctuations in mean receptor occupancy would be larger than difference between front and back. Gradient sensing may appear to be an impossible it such conditions but it must be remembered that the cell is averaging over time. For example, van Haastert

and Postma estimate that due to temporal averaging, cells can accurately read gradients when the noise is seven times the value of the mean receptor occupancy. Such an averaging would increase the reliability of the gradient sensing.

A more detailed examination the effect of noise on gradient sensing was performed by Ueda and Shibata [40]. The formalized the concept of "receptor gain" to be the response of the receptor to small fluctuations in ligand concentration. They defined the noise at the level of the receptor to be $\sigma^2 = \langle (R^* - \langle R^* \rangle)^2 \rangle$, where R^* is the activated receptor and the brackets indicate averaging over time. Thus the noise is simply the mean squared deviation of the activated receptor about its own mean. Then the noise can also be given by the relation,

$$\sigma^2 = g_R \langle R^* \rangle,$$

where g_R is the receptor gain. The gain quantifies the effect of small changes of ligand on receptor activation. It can be thought of as the sensitivity of receptor activation to changes in ligand. Importantly, the gain is a function of the ligand concentration, L, and is written as,

$$g_R = \frac{\Delta \langle R^* \rangle / \langle R^* \rangle}{\Delta L / L}.$$

Therefore, a reaction with higher gain displays greater sensitivity to small changes in L. Therefore, one strategy for the cell to sense shallow gradients is to have a high gain.

However, the noise is also proportional to the gain. Cells must then balance their sensitivity with their noise tolerance.

Endres and Wingreen examined the fundamental limits on gradient sensing set by diffusion [42]. They compared two models for the cell. The first model is the perfectly absorbing sphere. Here the cell is modeled as a sphere and completely absorbs every molecule of chemoattractant that it encounters and does not return it to the surrounding medium. Biologically speaking, this is similar to having either an infinite number of receptors with irreversible binding or a large number of receptors with reversible binding but some mechanism that prevents the return of the ligand to the medium. They point out that this could be accomplished via cell surface ligand degrading enzymes or through receptor internalization. The second model is the perfectly monitoring sphere. This cell perfectly counts every molecule that it encounters, but returns these to the medium.

Endres and Wingreen then derived an expression for the uncertainty in measuring concentration for each model. Interestingly for both cells, the uncertainty is independent of the magnitude of the gradient. However, the perfectly absorbing cell possessed an 8.6 fold lower uncertainty in measuring gradients compared to the perfectly monitoring cell. The sensitivity of the perfectly absorbing cell defines the lower limit of gradient measurement set by diffusion. They contend that the perfectly absorbing cell has higher sensitivity due to the fact that each molecule of ligand is only counted once, which is equivalent to saying that each measurement made by the cell is statistically independent of all others.

Using the model of the perfectly absorbing cell, they where able to accurately reproduce experiments on gradient sensitivity by van Haastert and Postma [38]. From this it is concluded that gradient sensing occurs at the threshold set by diffusion. This claim is remarkable because it suggests that the cell is a perfect gradient sensor. Although, *Dictyostelium* do have extracellular phosphodiesterases that degrade the chemoattractant cAMP, it is not clear how efficient they are at removing cAMP and therefore generating the conditions of a perfectly absorbing cell.

Although these theoretical efforts take different approaches and none recapitulates all the data available on gradient sensitivity, their conclusions are strikingly similar: chemotaxis appears to occur at the lower limits set by physical considerations. However, the value of all theoretical work must be evaluated within the limitations imposed by the assumptions made in deriving the model. For example, although it is known that chemoattractant receptors are uniformly distributed within the membrane, it has been clearly shown that the membrane of an amoeboid cell is not evenly distributed throughout the chemoattractant field [17]. This is due to the presence of a broad leading edge and a narrow uropod, which places far more receptive surface up the gradient than would be expected for a cell with perfectly elliptical morphology. Exactly how sensitive these models are to their assumptions is not currently known.

Rationale for Dissertation Work.

We seek to quantitatively study the movements of cells in an effort to isolate simple, overarching principles that provide insight into the regulation of cell motility. To do so, we will study both chemotaxis and non-directed motility looking for similarities or differences between these two forms of motility that are typically studied independently. Given that many pathways and processes are activated during both non-directed motility and chemotaxis, we believe that any real understanding of chemotaxis should be based on mechanisms general enough that they can also explain non-directed motility.

CHAPTER II

A COMPARISON OF CHEMOTAXIS IN LINEAR AND NONLINEAR GRADIENTS

Introduction.

Cell motility is an intriguing biological process requiring the direct coordination of multiple spatially and temporally complex subcellular processes, including signal transduction, cell-substrate adhesion, and cytoskeletal dynamics. Cell motility can be divided into two categories: nondirected, or isotropic, and directed motility. An example of directed motility of particular interest is chemotaxis. In chemotaxis, cells sense direction in chemoattractant concentration gradients via signal transduction and use this information to direct their motility to regions of higher concentration. In addition to being important during cancer progression, chemotaxis is essential for predation by cells of the immune system and the model organism *Dictyostelium discoidies*, where it also offers a developmental mechanism for multicellular structures to form from differentiating cells initially dispersed over long distances.

The identification of the signaling pathways responsible for chemoattractant gradient sensing is currently a vigorous area of research [35, 43, 44]. The PI3K-PTEN pathway responsible for the regulation of 3'-phosphoinositide (3'-PI) dynamics was identified as a strong candidate for regulating directional sensing in *Dictyostelium* [27, 45]. Cells lacking two PI3Ks were shown to have reduced cell polarity as well as a

reduced ability to maintain proper directionality during chemotaxis. Artificially targeting PI3K to the membrane or genetic deletion of PTEN led to increased pseudopodia formation and a poorly defined leading edge during chemotaxis, which in turn, resulted in reduced chemotactic efficiency. Furthermore, during chemotaxis PI3K was shown to localize to the leading edge membrane, whereas PTEN localized to the lateral and anterior cell membrane. This spatial distribution of PI3K and PTEN provided a mechanism to sharply regulate the spatial accumulation of 3'-PIs to the region of the cell membrane experiencing the highest concentration of the chemoattractant, cAMP. The leading edge localization of 3'-PIs was hypothesized to provide membrane binding sites for a host of signaling proteins that governed efficient F-actin assembly and pseudopod protrusion. Recently, we have shown that inhibition of PI3K by wortmannin in HL60 cells expressing CSCR2 resulted in reduced cell motility but normal chemotaxis in response to a gradient of CXCL8, and that wortmannin inhibition of PI3K impaired the ability of cells to re-orient their polarity and respond quickly to a change in the direction of the CXCL8 gradient [46, 47]. Similar results in a variety of cellular systems suggested that 3'-PI signaling was a rather general mechanism for regulating the cytoskeletal-dependent processes of cell polarity and chemotaxis [31, 48, 49].

In addition to directional sensing, the 3'-PI signaling system is also thought to play an important role in another aspect of gradient sensing, gradient amplification [11]. During gradient amplification, the weak external chemoattractant gradient is amplified into a strong internal signaling gradient, providing clear, reliable instruction from a noisy message. Gradient amplification is no mean feat considering that cells can consistently

sense and respond to concentration gradients so shallow as to occupy on the order of only 50 receptors, with minute differences in receptor occupancy across the cell body [50]. Importantly, both directional sensing and gradient amplification were shown to occur in cells treated with the actin polymerization inhibitor Latrunculin, where cells lose morphological polarity (and presumably F-actin-based cytoskeletal structure) [11, 51-53]. These results led to a model that the 3'-PI signaling system was independent of the cytoskeleton and therefore likely an instructive signal to the F-actin-based cell protrusions that play a key role in displacing the cell body [54].

Increased scrutiny has led to a more complex picture of the role of 3'-PIs in *Dictyostelium* cell motility and chemotaxis. A detailed analysis of pseudopod dynamics during chemotaxis suggested that 3'-PIs regulated the frequency, but not the directional accuracy, of pseudopod extension calling into question the role of 3'-PIs in directional sensing [55]. Subsequently, a *Dictyostelium* mutant lacking all five known type I PI3Ks was reported to undergo chemotaxis with "near wildtype efficiency", further questioning the role of 3'-PIs in chemotaxis [34]. Curiously, the speed of random motility, but not chemotaxis, is reduced in the pentuple knockout, suggesting that 3'-PIs might only play a role in regulating basal cell motility. Likewise, a detailed comparison of pseudopod dynamics during isotropic and directed motility found that *pten*- cells had an increased number of lateral pseudopodia, a defect that was manifested to the same degree in both of these paradigms of cell motility [56]. The similarity of the defect in both conditions led to the conclusion that PTEN function is largely independent of receptor activation. Finally, PI3K (and reporters for 3'-PI accumulation) have been

shown to spontaneously localize to the membrane independent of G-protein-dependent constitutive activity of the chemoattractant receptor [57]. Similarly, PTEN was observed to delocalize from the membrane at sites of random pseudopod extension. Although a clear role for 3'-PIs in isotropic motility and chemotaxis has yet to emerge, it is becoming apparent that the precise function of 3'-PIs in regulating cell motility is more complex than originally supposed.

We have investigated a specific role for receptor-regulated 3'-PI signaling in chemotaxis by measuring directional accuracy and speed for *wt*, *pi3k1/2-,* and *pten-* cells in chemoattractant gradients produced by micropipette and a microfluidic device. In the micropipette assay, a nonlinear gradient with radial symmetry is produced, which a cell chemotaxing towards areas of higher concentration would experience as an increasingly stronger directional signal. In contrast, the gradient produced by the microfluidic device we used is linear, *i.e.*, it has a constant steepness in one direction and is translationally invariant in the other. Comparison of chemotaxis as a function of position in the differing gradients revealed that only *wt* and *pi3k1/2-* cells are capable of increasing directional accuracy as they approached regions of higher chemoattractant concentration in the nonlinear micropipette assay, indicating that the degradation of 3'-PIs by PTEN is required for cells to capitalize on the stronger directional signal offered by increasingly steeper concentration gradients. Similar analysis of cells in a linear gradient suggests that the change in gradient steepness in the micropipette assay is responsible for the increase in accuracy, as all three genotypes were incapable of increasing their accuracy as they moved into regions of higher concentration. In the nonlinear gradient,

both *wt* and *pi3k1/2*- cells were capable of increasing their speed as they approached the micropipette, while only *pi3k1/2*- and *pten*- were capable of doing so in the linear gradient. Examination of the relationship between the direction and magnitude of chemotactic movements revealed that these parameters, although often reported as independent measures of chemotaxis, are in fact coordinated by the cell in both linear and nonlinear gradients to increase chemotactic efficiency. Both *pi3k 1/2*- and *pten*- cells had an overall decreased ability to coordinate their speed and directional accuracy, while *pten*- cells had an impaired ability compared to *wt* and *pi3k 1/2*- to increase their coordination as they moved into regions of higher concentration in the micropipette assay. These results suggest that receptor-driven 3'-PI signaling plays a key role in coordinating speed and accuracy, thereby increasing chemotactic efficiency.

Methods.

Cell culture and preparation.

Cells were cultured axenically in HL5 supplemented with glucose and penicillin-streptomycin. For chemotactic competence, cells were shaken for a maximum of two days, washed three times in Na/K phosphate buffer, and resuspended for a final density of 5 x 10^6 cells/mL in 30 mL of buffer. cAMP was delivered every six minutes for five hours. Cells were plated (micropipette assay) or injected (microfluidic device) and allowed to adhere and disperse. Recording commenced no more than six and a half

hours after the pulsing began. *pten-* cells were obtained from the *Dictyostelium* Stock Center.

Imaging and cell tracking.

All imaging was done on a Nikon TE-30 inverted microscope using 20x DIC optics (Nikon), NA=1.4, and a CoolSnap camera. Using 2-by-2 binning resulted in a field 430 µm wide and 321 µm high and a pixel density of 2.6 pixels per µm ^{2}. Cells were imaged for one and a half hours at a frequency of 1/3 Hz. The following criteria were established to ensure consistency throughout experimentation and analysis: 1) Cells were tracked for a minimum of 100 frames (*i.e.*, 300 seconds). 2) Cells were only tracked if the entire cell body remained completely within the field of view. 3) Cells that came in physical contact with other cells were avoided. 4) Care was taken to avoid cells that were closely following other cells to eliminate any influence from streaming or cell-to-cell signaling. Tracking was done using the Metamorph (Molecular Probes, OR) "track objects" function and logged to Excel (Microsoft, Redmond, WA). For more data regarding the sample sizes and tracking times, see Table 1.

To obtain estimates of the concentration field produced by the micropipette, we first imaged dilute, uniform concentrations of fluorescein (MW 332.2) to determine the range for which its fluorescence was linearly related to imaged intensity. We then imaged a gradient resulting from highly concentrated fluorescein. The gradient was rapidly produced with intensity values within the predetermined linear range. An

exponential curve was found to fit the data obtained from linescans of the original images with minimal error.

Microfabrication and Device Operation.

All microfabrication was performed using soft lithographic, rapid prototyping methods [58, 59]. Briefly, SU-8 150 (Microchem, Newton, MA) was deposited on dried, acetone-cleaned silicon wafers and spun to a thickness of approximately 100 μm. Film masks were printed at a resolution of 3556 dpi. After UV exposure and baking, the remaining photoresist was washed away, leaving a positive master. Devices were created by pouring mixed and degassed PDMS:PDMS crosslinker at a ratio of 1:10 over a master in a 30 mm petri dish. After incubation for at least two hours at 80 degrees C, the PDMS was removed, devices trimmed to size, and channels punched. After plasma treatment for ten seconds, PDMS devices were then bonded to glass. The resulting devices ranged from 100-185 μm s tall with a chemotaxis chamber 500 μm wide.

Devices were operated using 1 mL syringes driven by a Harvard syringe pump. To maintain consistent shear flow across numerous experiments, the programmed flow rates were adjusted according to [60].

Data analysis.

Our definition of accuracy is a transformation of the direction, θ, of a chemotactic movement as measured on the interval [0°-180°] relative to the direction of the gradient and was defined as: $a(t) = -1/90 \bullet \theta(t) + 1$. As for the more familiar

chemotactic index, defined as $CI(t) = \cos(\theta(t))$, the accuracy transformation provides an index ranging between –1 and +1. However, the accuracy index used here differs importantly from the chemotactic index in that it is a linear transformation of angle values and therefore does not contain the distortions introduced by the cosine function. Therefore, the linear transformation is preferred for statistical analysis. All analysis done here was with data from three second sampling intervals.

Mean accuracy, speed, and coordination were compared by a two-way ANOVA using, in the case of chemotaxis, concentration profile and genotype as factors. After obtaining evidence that concentration profiles and genotypes were significantly different by two-way ANOVA, genotypes were compared using Bonferroni t-test. All mean values from the simulations of coordination were compared using ANOVA. Regression coefficients and their associated errors were obtained by regressing the mean speed, accuracy, or coordination averaged over ten micron intervals using the Matlab function robustfit.m. *t* values assessing the significance of the slope and y-intercept coefficients (or differences between them) and their associated *p* values were calculated according to [61]. All analyses were done in Matlab (Mathworks, Natick, MA).

Simulation of coordination.

Stochastic simulations of coordination were performed in Matlab as follows. The *n* pooled chemotactic speeds and directions of *wt* cells in the micropipette assay were separately ranked by increasing speed and accuracy, respectively. For every discrete time step of the simulation, *t*, a uniformly distributed random integer, *r*, with a value

between one and *n* was generated and the speed with rank *r* was chosen from the experimental distribution. The accuracy of the movement at time *t* was chosen to be either the direction with rank *r* or an independently chosen rank. A free parameter of the model, λ, defined to be between zero and one, determines the fraction of the time that the model randomly chooses directions with the same rank as the speed, and therefore, the degree of coordination between speed and direction in the simulation. For each degree of coordination in the simulation, 80 cells were simulated for 500 time steps each.

Results.

Description of the chemotaxis assays.

Using a micropipette to create a chemoattractant concentration gradient, it was recently shown that *wt* cells increase their directional accuracy as they approach the gradient source [62]. In the standard micropipette assay, the chemoattractant concentration falls off nonlinearly with increased distance from the micropipette, creating for a cell approaching the gradient source a gradient of ever increasing steepness and mean concentration (Figure 6A). As 3'-PI signaling has been shown to be involved in adaptation to mean concentrations and to amplify the chemoattractant gradient [11, 51] and to regulate directional accuracy [45], we hypothesized that two features of this experiment were essential for this result: 1) the ever-increasing steepness, or the nonlinearity, of the chemoattractant gradient, and 2) regulated 3'-PI signaling as required for the amplification of the consistently stronger gradient and the

regulation of leading edge F-actin dynamics. We resolved to test this notion through the comparison of *wt*, *pi3k1/2-*, and *pten-* cells in the micropipette assay and in a linear gradient generated by the microfluidic device (Figures 6B and C). The gradient in the micropipette assay was created by free diffusion of the chemoattract cAMP from a micropipette containing ~30 μL of 100 μM cAMP. With this concentration, a nonlinear gradient with a mean concentration in the low nM range was created within ~250 μm of the micropipette and cells of all three genotypes were capable of sensing and responding from distances of at least 220 μm. The exact concentration profile resulting from the diffusion from the pipette tip at the bottom of the dish depends upon a number of geometric and temporal factors; the curve shown in Figure 6A is consistent for *x* > ~10 μm with the expected steady-state, $1/r$ concentration profile for a constant-concentration point source [63]

$$C(x) = \frac{C_o}{r} = \frac{C_o}{\sqrt{x^2 + y^2 + z^2}} \quad ,$$

where the bottom of the dish is the $x-y$ plane and z is the vertical distance. When the pipette is first inserted into the dish, the falloff will be transiently steeper than this, since the chemoattractant will not yet have diffused out into the bulk fluid. The microscope sums the fluorescence intensity over a range of z values, so that the observed intensity profile such as Figure 6A is obtained by integrating the concentration from $z = 0$ to $Z_{\max}$ to produce an intensity profile given by

$$I(x) = I_o \log\left(\frac{y_{\max}}{x} + \sqrt{1 + \left(\frac{y_{\max}}{x}\right)^2}\right) \quad .$$

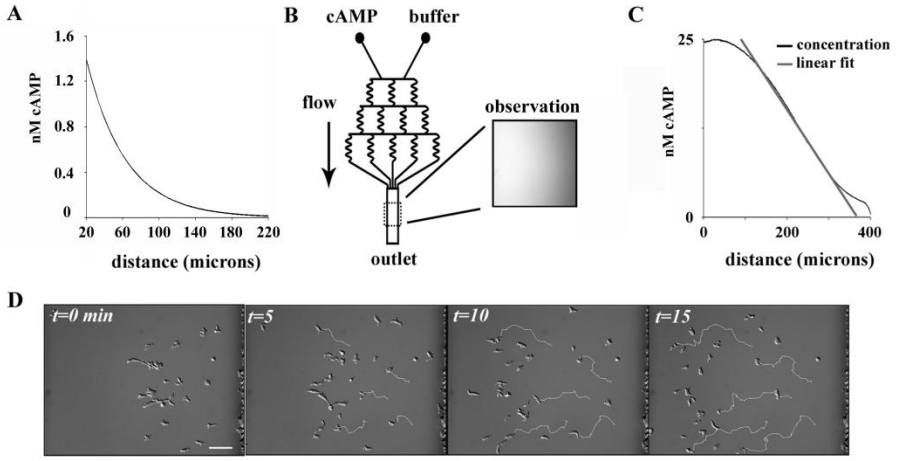

Figure 6 **Experimental and analytical paradigm to measure directed and persistent random motility.** A) Quantitation of fluorescein (MW 332.3) diffusing from a micropipette reveals the nonlinear concentration profile in the assay. B) Schematic of the microfluidic device used in the study where manipulation of the flow into the two inlets (labeled cAMP and buffer) gives the ability to produce stable concentration gradients. Inset, image of fluorescein fluorescence in the device. C) Quantification from a line scan of fluorescein image in B detailing experimental control over chemoattractant profiles. Flowing buffer and cAMP at identical flow rates creates linear chemoattractant concentration gradients for chemotaxis that are stable over experimental time-scales (<90 minutes). D) Time-series showing the chemotaxis of *wt* cells in the microfluidic device when exposed to a linear cAMP gradient of 50 pM/μm cAMP with a midpoint of 12.5 nM (concentration increases from right to left and flow is from top to bottom). For clarity, five cells were chosen and their respective tracks are shown in white.

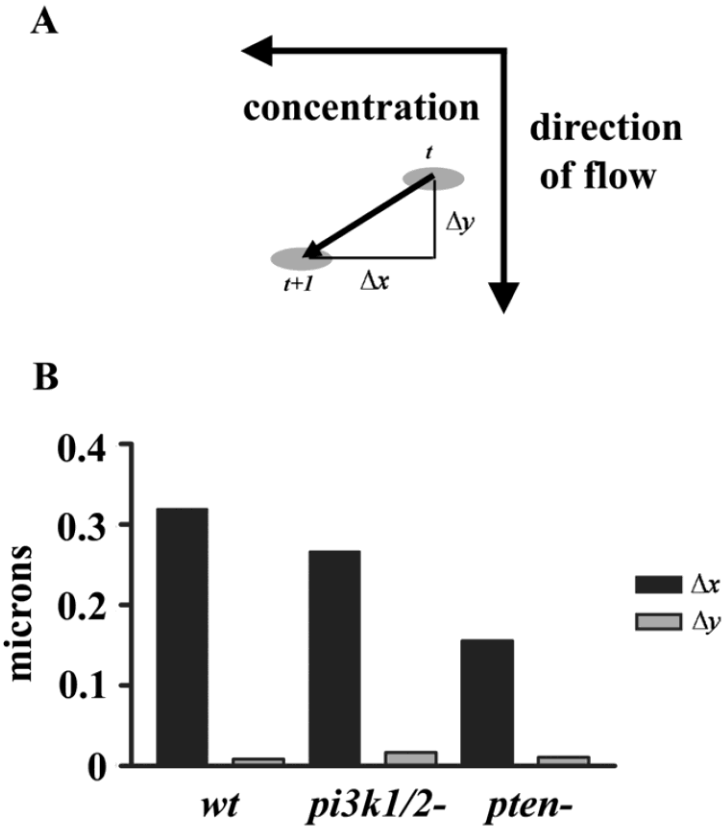

Figure 7**. Comparison of the magnitude of movement in the direction of the gradient with movement in the direction of the flow.** A) Diagram detailing the geometry used in the measurements. Positive displacements are in the direction of the gradient or flow. B) Mean displacements in the direction of the gradient and flow for the three cell lines in the study.

To determine the optimal conditions in the microfluidic device, a pilot study revealed that the chemotaxis of *wt* cells was the most efficient in a gradient of 50 pM/ μm cAMP with a midpoint of 12.5 nM cAMP (data not shown). For an example of the chemotaxis of *wt* cells in these conditions, refer to Figure 6D. These conditions are in good agreement with those found in [15]. The stability of the gradient in the device is driven by fluid flow, which also creates shear force on adherent cells perpendicular to

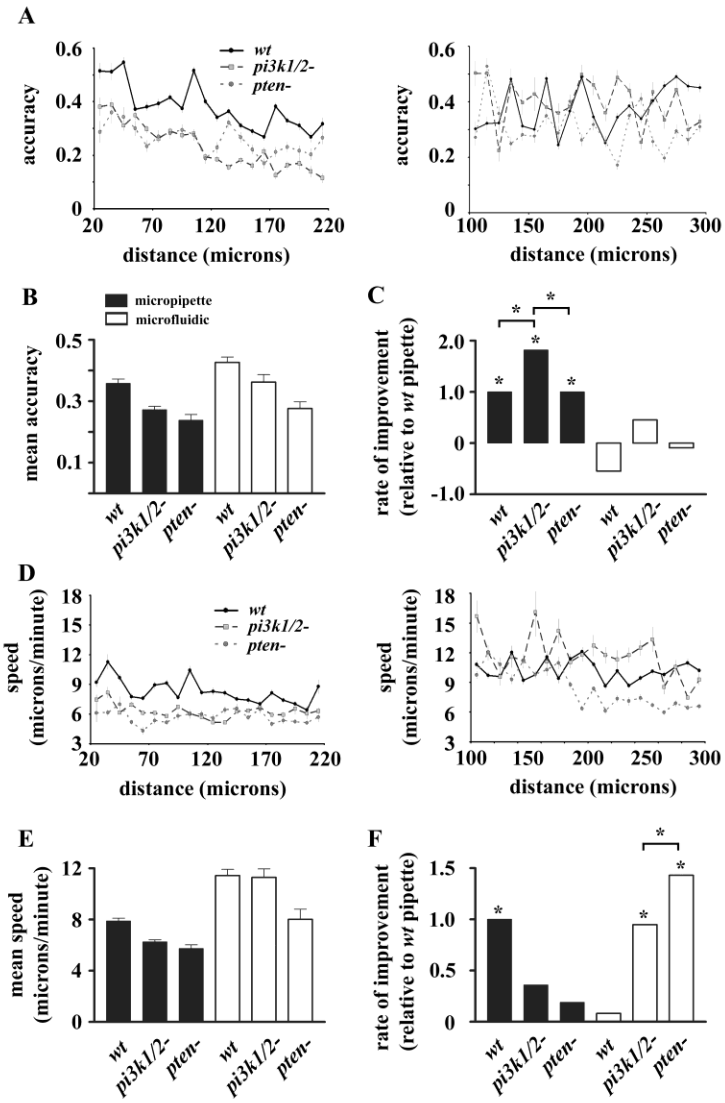

Figure 8 **Chemotactic accuracy and speed in linear and nonlinear concentration gradients.** The chemotactic accuracy (A) and speed (D) of the three genotypes versus distance from the highest concentration in the nonlinear gradient (left) and linear gradient (right). Mean accuracy (B) and speed (E) for *wt*, *pi3k1/2*$^{-}$, and *pten*$^{-}$ in the micropipette (nonlinear) and microfluidic (linear) assay, respectively. Statistical comparison of the rate of improvement of accuracy (C) and speed (F) in the micropipette assay and the linear region of the microfluidic device. For comparison, the rate of increase in each chemotactic parameter was normalized to the rate of *wt* cells in the micropipette assay. Stars represent statistically significant differences at $p < 0.05$.

the direction of the gradient [60]. By varying the flow, we determined that a flow rate of 1.4 μL/minute produces a stable gradient had no apparent effects on motility (see Figure 7). At this low rate, the estimated 10 pN shear force is approximately one-half as large as that required to initiate Ca^{2+} regulated, shear flow-driven motility and considerably lower than that shown to activate the 3'-PI signaling pathway in vegetative cells [64, 65]. Furthermore, chemotaxis in higher shear forces (40pN) also showed no obvious directional bias by flow (data not shown). For all three genotypes, cells were more accurate and faster in the linear gradient than in the micropipette assay (Figures 8B and E).

Accuracy in linear and nonlinear gradients.

To test the role of 3'-PIs and chemoattractant concentration profile in increasing efficiency with increased proximity to higher concentrations, we plotted the directional accuracy and speed (Figure 8A and D, respectively) of *wt*, *pi3k1/2*, and *pten*$^-$ cells chemotaxing in linear and nonlinear gradients. The directional accuracy ranges from -1, for movements directly away from the highest concentration, to +1 for movements directly toward the highest concentration (see methods for complete definition). As the gradient steepness increases with increased proximity to the highest concentration in the micropipette assay, distance is used as a proxy for gradient steepness. To address the magnitude and statistical significance of any potential trend, we performed linear regression for each measure of chemotactic behavior as a function

Table 1. Sample sizes, tracking times, and mean measures for each genotype in every condition tested. Values are for mean with standard error in parentheses except for tracking time, which is shown as mean with the standard deviation in parentheses. *N* and *n* are the number of experiments and the number of cells, respectively, for the given genotype in a particular condition.

	micropipette	microfluidic device
wt		
N=	6	5
n=	99	61
mean tracking time (minutes)	10.91 (4.94)	21.15 (11.82)
pi3k1/2-		
N=	9	4
n=	124	28
mean tracking time (minutes)	14.06 (11.46)	18.09 (12.88)
pten-		
N=	6	6
n=	52	41
mean tracking time (minutes)	16.49 (10.54)	31.51 (18.70)

of distance from the micropipette (see Table 1 for regression coefficients). The slopes were compared statistically as measures of a genotype's rate of improvement with increasing proximity to higher concentrations. Statistically significant increases in directional accuracy were seen in all three genotypes tested (Figure 8C). Although *pi3k1/2-* cells were capable of increasing their accuracy to a greater degree than *wt* and *pten-,* both *pi3k1/2-* and *pten-* cells displayed an overall lower chemotactic accuracy and

speed in the micropipette assay. In the micropipette assay only *wt* was capable of increasing their speed as they experienced steeper concentration gradients. The lack of increased speed in *pi3k1/2*-and *pten*- cells reveals that proper regulation of 3'-PIs is required for increasing chemotactic speed with increased proximity to the micropipette.

To verify that the improvement in directional accuracy by all three genotypes was due to the varying gradient steepness in the micropipette assay, we repeated our analysis of chemotactic accuracy and speed as a function of distance from the highest concentration in the linear gradient where the gradient steepness is held constant. Chemotaxis over distance in the shallow, linear gradient was considerably more variable than in the micropipette assay, and no genotype showed a statistically significant ability to increase accuracy as it approached regions of higher concentration (Figures 8A and D). Although *wt* cells in the linear gradient apparently decreased their accuracy as they moved into regions of higher concentration (Figure 8C), this negative relationship was not statistically significant. Thus, the increases in accuracy by cells seen in the micropipette assay are likely due to either the rate at which the mean concentration increases in the different assays or the ever-increasing gradient steepness experienced by a cell. We have not yet addressed the question of whether any of the observed behavior was the result of the radial nature of the diffusion from the micropipette – since a lateral or directional error in a cell trajectory could produce a larger change in concentration for the pipette than would a corresponding error in the translationally invariant microfluidic device. This issue could be resolved by using a microfluidic

gradient generator that produced non-linear, translationally invariant gradients (Campbell and Groisman, 2007).

Speed in linear and non-linear gradients.

Interestingly, despite having mean speeds lower than *wt* (Figure 8E), both *pi3k1/2*- and *pten*- cells, unlike *wt*, were capable of increasing their speed with increased proximity to the highest concentration in the linear gradient (Figure 8F). Thus, for the mutants with impaired 3'-PI signaling, increases in speed are not dependent upon the presence of a nonlinear gradient. This discrepancy may indicate that the mechanism relating speed to gradient strength may be uncoupled in 3'-PI signaling mutants.

Coordination between speed and accuracy determines chemotactic efficiency.

Speed and direction are the two most commonly utilized measures of chemotactic efficiency (for example, see [34, 55, 66]). It is likely that in considering these two parameters separately (and thereby implicitly assuming that they are independent of each other) there is a possibility of neglecting the prospect that the cell might coordinate its direction and speed to increase the efficiency of chemotaxis. To examine how these two measures of chemotactic efficiency may depend upon one another and explore how that potential dependence may differ between *wt* and 3'-PI

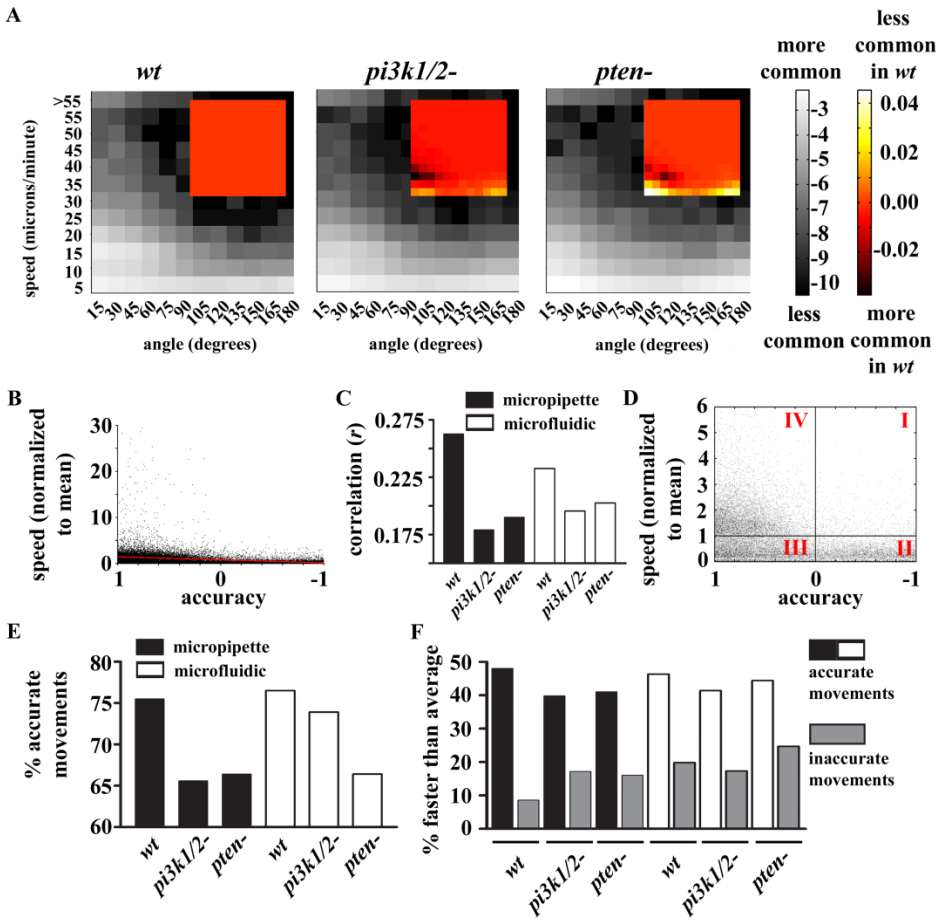

Figure 9 **During chemotaxis, accurate movements tend to be faster movements.** A) Two-dimensional histograms displaying the log of the probability that a cell will make a movement during chemotaxis in the micropipette and microfluidic assay with a particular angle (x-axis) and speed (y-axis) represented in gray-scale. Speed values are separated in bins 5 μm/minute wide while angle is in bins 15° wide and each bin is labeled with the upper limit for that bin. The heat-mapped insets show the difference between a given mutant and *wt*. Doubling and halving the bin widths had no appreciable effect on the general conclusion. Similar patterns can be seen in 2- histograms of movements from the microfludic device. B) Scatter plot of the accuracy of *wt* movements versus their speed after normalized to each individual cells mean speed. A linear fit (red line) indicates the correlation between accuracy and speed. C) Correlation coefficients between each genotypes accuracy and normalized speed (as in B). Each correlation was found to be significant at $p<0.05$ level. D) A magnification of the plot from B. This plot, containing >99% of the total data, can be divided into 4 regions, labeled I,II,III,IV, that describe the accuracy and speed of the cell (see text). E) Percent of movements from each genotype with positive accuracy (quadrants III and IV in D). F) Percent of accurate and inaccurate movements with faster than average speeds.

signaling mutants, we computed the two-dimensional probability distributions of speed and direction as measured between 0-180° (with 0° being perfectly accurate and 180° being perfectly inaccurate) for *wt* and both mutant cell lines during chemotaxis in the micropipette and microfluidic assay (Figure 9). The full range of angles and speeds were divided into bins with widths of 15° and 5 μm/minute, respectively, and labeled with the upper-limit of each bin. A gray-scale colormap was used to depict the probability that a cell of a given genotype would make a movement of a particular range of speed and angles. Although the most common movements in all three cell lines fall within the 0-5 μm/minute range, a fair number also occurs in the range of 5-20 μm/minute. Of those movements that were faster than typical, the majority were associated with directions that brought the cell closer to the micropipette (*i.e.*, angles < 90°). Therefore the majority of the probability gathers in the lower left-hand quadrant of each genotype's distribution indicating dependence between the speed and direction of movement. In biological terms, cells tend to adjust the magnitude of their movements according to their accuracy (and/or vice versa).

To provide a comparison between the distributions of the mutants to *wt*, the two-dimensional distribution of *wt* cells was subtracted from each respective mutant and presented as insets in Figure 9. Two regions contrasting the coordination of *wt* and the mutants can be seen in the difference distributions. First, for both mutants in both assays there is a substantial decrease in the faster (*i.e.* > 5 μm/minute) movements associated with accurate directions and a corresponding increase in slower (0-5 μ

m/minute) movements also associated with accurate directions. This shifting of probability from higher speeds to lower speeds while directional accuracy remains roughly constant, is consistent with the observation that the largest defect in *pi3k 1/2*- cells or *wt* cells treated with the PI3K inhibitor LY429009 being a reduction in speed but not directional accuracy, and is suggestive of a role of 3'-PIs in regulating basal cell motility [66]. The role of PI3K in sensing change in gradient direction has been demonstrated by blocking PI3K with wortmannin [46], but it is not yet clear whether this treatment also affects chemotactic accuracy between linear and radial gradients. However, a second region of difference can also be seen as an increase in large, inaccurate directions, suggesting a role for 3'-PIs in directional accuracy. Thus, *Dictyostelium* cells coordinate their "choice" of direction with their "choice" of speed in a manner that is dependent, in part, on 3'-PI signaling.

For a quantitative understanding of the relationship between speed and direction, we first determined the mean speed of each cell and used this to normalize the speed of all its movements. The normalized speed of each movement was then plotted versus its accuracy for all three genotypes in each experimental assay (for an example, see Figure 9B). Correlation coefficients were computed and their significance ascertained. The magnitudes of the correlation coefficients are plotted in Figure 9C. All cell lines in both assays displayed statistically significant correlation between their accuracy and their normalized speed, although the correlation coefficients for both mutants were considerably reduced compared to *wt*.

In addition to the presence of correlation, the scatter plots of normalized speed versus accuracy further exemplify the argument that accurate movements tend to be faster movements. The plot can be divided into the following four regions, region I with above inaccurate directions and above average speeds, region II with inaccurate directions and below average speeds, region III containing accurate movements with below average speed, and region IV with accurate movements with above average speed (Figure 9D). Examination of the distribution of the data points with above average speed suggested there were considerably more above average speed movements that were accurate than inaccurate. However, as there are also far more accurate movements than inaccurate movements, regardless of speed (Figure 9E), comparisons solely between accurate and inaccurate above average speed movements could be misleading. To account for the fact that there are more accurate than inaccurate movements, we determined the percentage of total accurate movements that also had above average speed, and similarly, the percentage of total inaccurate movements that also had above average speed (Figure 9F). With this analysis, it can be seen that accurate movements were 2-5 times more likely to be faster than average as compared with inaccurate movements.

To better demonstrate the consequences of the interdependence between speed and direction on chemotactic efficiency and the usefulness of our definition of coordination, we performed simulations of chemotaxis where the coordination between speed of cell movement and the directional accuracy could be varied. For each relative level of coordination, cell tracks, the means, and the distributions of speed and angle

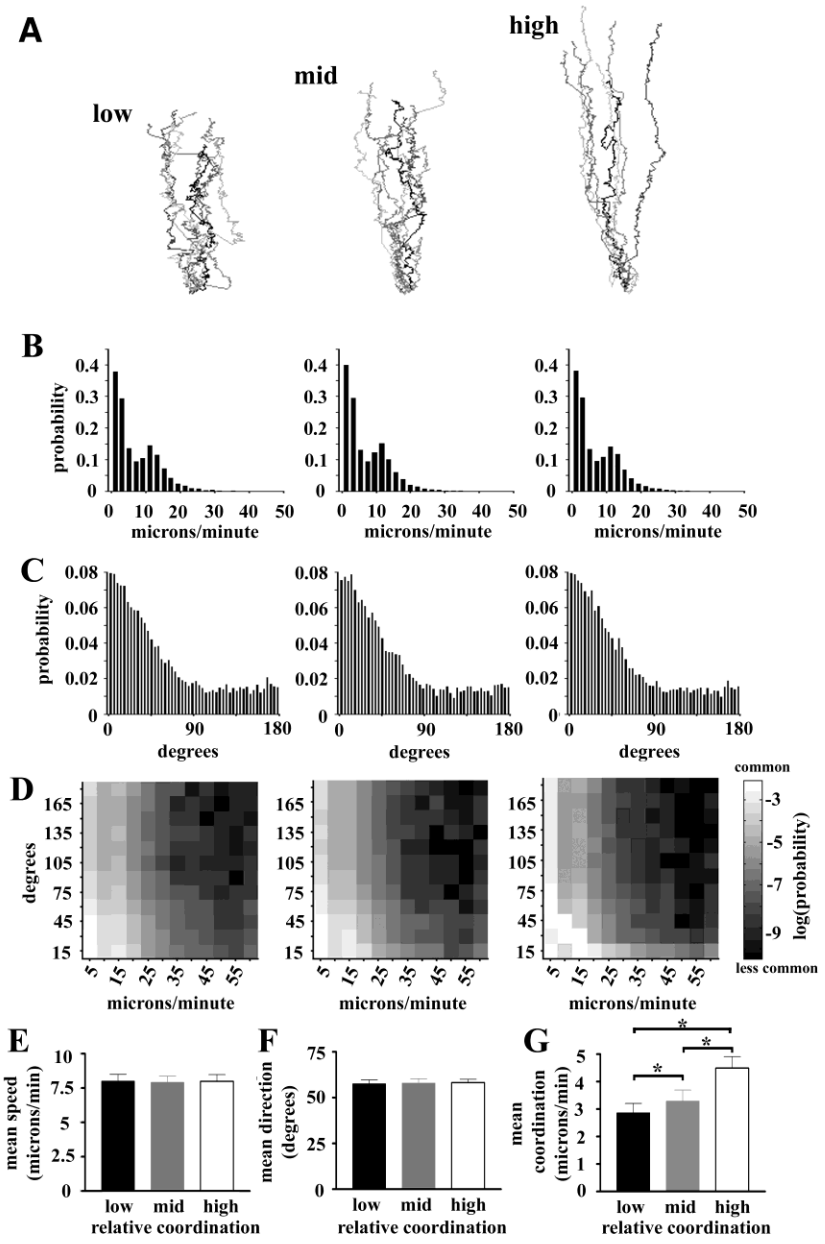

Figure 10 **Simulations of coordination reveal its effect on chemotactic efficiency.** A) "Tracks" of cells from a stochastic simulation of chemotaxis with varying degrees of coordination between directional accuracy and speed. B and C) The probability distribution of the speed and direction, respectively, of cells in A. D) The two-dimensional probability distributions reveal the dependency of directional accuracy and speed in the simulations in A. E and F) Mean speed and direction for each simulation in A. G) Mean coordination index for each simulation. The stars indicate differences at the *p<0.05* level by Bonferroni t-test following ANOVA.

were determined (Figure 10). It is easy to see that the cell tracks displayed in Figure 10A qualitatively show widely varying degrees of chemotactic efficiency. As coordination between speed and accuracy is increased, the simulated “cells” produced tracks that became less tortuous with fewer and fewer “runs” of inaccurate movements and the overall distance covered was increased. It should be noted that these apparent differences exist despite the fact that the probability distributions of the speed and direction of each simulation, considered separately, fails to suggest any significant differences in the different simulations (Figure 10B and C). Only the two-dimensional probability distributions (Figure 10D) were capable of revealing any difference between the simulations as more probability gathers in the lower lefthand quadrant as the degree of coordination is increased. Most interestingly, statistical comparison of the mean values of speed or angle reveals the inadequacy of population means to differentiate the striking variability in chemotactic efficiency seen in the tracks, as the simulations proved to be statistically identical (Figure 10E and F).

Given that speed and directional accuracy alone proved to be inadequate to describe chemotactic efficiency, we developed a measurement that could combine information on the speed with the direction of cell movement. This measurement, called the coordination index, was obtained by multiplying the accuracy index which, again, ranges between –1 and +1 (with –1 being a movement in directly away and +1 being a movement directly towards the highest concentration) by the speed of that particular movement. The coordination index, therefore, weighs the speed of the cell movement according to the accuracy of the movement. An additional desirable property

of the coordination index is that negative values are allowed, unlike speed, which, by definition, is always positive. Statistical comparison of the mean coordination index of the simulations in Figure 10A proved the simulations to be significantly different from each other (Figure 10G). This result underscores the limitations of considering speed and accuracy separately and highlights the usefulness of the coordination index to describe chemotactic efficiency.

Coordination in linear and non-linear gradients.

As chemotactic efficiency is dependent upon direction *and* speed, and accuracy is known to increase as cells approach regions of higher concentration in the micropipette assay, we asked if the coordination between speed and accuracy also increased in a similar manner. As for both speed and accuracy, the mean coordination of all cells in the linear gradient was higher than in the micropipette assay. For both gradient profiles, *wt* cells had significantly higher coordination compared to *pi3k1/2*- and *pten-,* while *pi3k1/2*- had higher coordination than *pten*- (Figure 11A). Examination of the coordination as a function of distance from the micropipette revealed that not only were *wt* cells capable of increasing their accuracy and speed as they approached the micropipette, but they were also capable of increasing the coordination between accuracy and speed (Figure 11B). Both mutants also revealed an ability to increase their coordination as they approached the micropipette although their ability to do so was significantly reduced compared to *wt*. No genotype tested was capable of improvements in coordination as they approached the highest concentration in the

linear gradient and in fact, *wt* cells showed a significant decrease in coordination over distance. This suggests that nonlinear gradient generated in the micropipette assay was required for improvements in coordination. Thus, assuming that the sensing system is not saturated in the regions measured here, the regulation of 3'-PI signaling is required for increases in the coordination of accuracy and speed by cells during chemotaxis in nonlinear gradients.

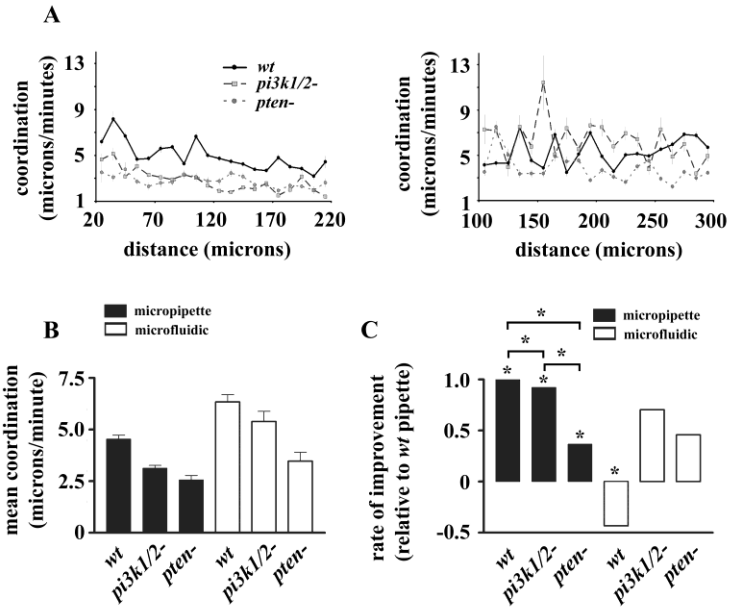

Figure 11 **Coordination in linear and nonlinear concentration gradients.** A) Coordination versus distance from the highest chemoattractant concentration present in the nonlinear gradient (left) and linear gradient (right). B) Comparison of the mean coordination of the three genotypes in the linear and nonlinear gradients. C) Statistical comparison of the rate of improvement of coordination in the micropipette assay and the linear region of the microfluidic device. For comparison of the increase in the coordination, the rate of increase was normalized to the rate of *wt* cells in the micropipette assay. Stars represent statistically significant differences at $p < 0.05$.

Discussion.

It was recently shown that *wt* cells increase their directional accuracy as they approach the micropipette [62]. Our data corroborate and extend these findings by showing that *wt* cells also increase their speed and the coordination between the speed and direction as they approach the gradient source. Given the nonlinear nature of the concentration gradient generated in the micropipette assay, a cell moving towards the micropipette would experience a gradient whose steepness would be consistently increasing. According to the model where the steepness of the 3'-PI signaling gradient is directly related to the steepness of the chemoattractant gradient, we hypothesized that an ever steeper chemoattractant gradient would result in ever steeper 3'-PI signaling polarity and more efficient chemotaxis. As they approached the micropipette, *wt* and *pi3k1/2*- cells were capable of increasing their directional accuracy. *Dictyostelium* possess five type I PI3Ks, so the improvement in chemotaxis seen here most likely results from the residual PI3K activity in the *pi3k1/2*- mutant. Chemotactic efficiency in the microfluidic device was statistically higher than in the micropipette assay. This is likely due to the increased stability of the concentration gradient present in the microfluidic device. In the linear gradient the chemotactic ability of all three genotypes over distance was more erratic (Figures 2A and D and 4B), and no increase in accuracy or coordination was seen for any genotype. A similar result was seen in [67] when qualitatively comparing the movements of immune cells in linear and nonlinear gradients, while our quantitative examination suggests that the change in gradient

steepness or mean concentration experienced by a cell can account for the increased erratic behavior in the linear gradient.

There are at least four possible explanations for differences in the regulation of chemotactic efficiency in linear and nonlinear gradients: 1) a temporal effect where the directional accuracy and speed of a cell improves during a prolonged chemotactic run, 2) a temporally-induced chemokinetic effect where changes in mean concentration result in changes in motility, 3) changes in gradient steepness, and 4) the effects of the radial concentration profile leading the changes not only in the magnitude of the local gradient but also its direction. Although there does qualitatively appear to be an increase in speed and accuracy of a cell over time (data not shown), it is likely that this phenomenon is not responsible for the increased accuracy seen in the micropipette for several reasons. For example, an increase in accuracy over time should result in increases in accuracy in the linear gradient as well, but we found no evidence of any such behavior. Also, in the micropipette assay (as well as the linear gradient), the initial distributions of cells were thoroughly scattered at various distances from the highest concentration, which would tend to obscure any effect that temporal increases would have on measures of accuracy as a function of distance. With the current study it is impossible to rule out a temporally-induced chemokinetic effect, as the difference in the rate of change in mean concentration, by definition, differs between the two assays. Although *Dictyostelium* has been shown to be capable of sensing purely spatial chemoattractant gradients [11] it must be noted that chemokinesis in *Dictyostelium* has been measured for cAMP concentrations ranging from pM to μM and the mean speed

was only appreciably increased over buffer in 10nM cAMP [68]. Either as the result of increased gradient steepness or a novel temporally-induced chemokinetic effect, the increases in accuracy and coordination seen here clearly indicate a receptor-dependent 3'-PI regulation of chemotaxis. Comparison of the radial gradients with a $1/r$ profile with translationally invariant $1/x$ gradients would require more complex microfluidic gradient generators than the ones used in these experiments [69].

It has been shown that eukaryotic chemotaxis displays characteristics of a biased random walk, where individual movements are, on occasion, directionally random, but over the long term, the directions are biased enough to produce efficient chemotaxis [62, 67, 70]. Our detailed examination revealed that during chemotaxis, *Dictyostelium* cells are capable of coordinating the speed of their motility with the direction such that faster than average movements tend to be accurate in direction. To better capture chemotactic efficiency, we have introduced a new descriptive parameter, the coordination index, capable of describing the coordination between speed and directional accuracy. A similar definition was suggested but not applied in [66], as best representing chemotactic efficiency. Coordination, while not absolutely required for chemotaxis, nonetheless serves to de-emphasize directionally inaccurate movements and increase the efficiency with which the cells are capable of reaching their destination. We hypothesize that coordination comes about as a result of directionally biasing the extension and/or extending the lifetime of cytoskeletal projections during chemotaxis. Interestingly, *pi3k1/2*- and *pten*- cells both showed a decreased ability to coordinate their speed and accuracy, suggesting a role for 3'-PIs in regulating

coordination. Consistent with this notion, both *pi3k1/2*- and *pten*- cells, unlike *wt*, were capable of increasing their speed in the microfluidic device. We interpret this ability that is present in mutants but not in *wt* to be a further indication of the loss of coupling between speed and direction following the dysregulation of 3'-PI signaling.

Recent attempts to understand theoretically the motile response to eukaryotic gradient sensing have only focused on explaining the directional accuracy of the cell [62, 67, 70]. Despite the impressive results in explaining the directional component of eukaryotic chemotaxis provided by these efforts, our data argues that a more complete model must take into account speed in addition to directional accuracy. Introducing speed into a model that relates the chemoattractant gradient to the motility of the cell introduces requires the introduction of time into the model. This is subject of ongoing work.

The molecular mechanisms responsible for chemoattractant gradient sensing and the manner in which sensory pathways integrate with cytoskeletal dynamics are, in many ways, the largest open questions in eukaryotic chemotaxis. We examined the role of the 3'-PI signaling pathway, a leading candidate in regulating gradient sensing by comparing the movement of *wt* and mutant cells with defects in 3'-PI signaling in linear and nonlinear gradients. We found that cells coordinate speed and directional accuracy during chemotaxis to raise chemotactic efficiency, and that their ability to take advantage of increased directional strength in a nonlinear gradient and increase both accuracy and coordination as they approach higher concentrations required the degradation of 3'-PI by *pten*-. We suspect the coordination of speed and accuracy during

coordination to be complex and regulated by multiple, potentially redundant pathways, as we have shown here that receptor-driven 3'-PI signaling, in part but not *in toto*, regulates the coordination of chemotaxis in *Dictyostelium*. We hypothesize that the coordination of speed and directional accuracy is likely to be universal for chemotactic cells as higher overall chemotactic efficiency is likely to offer a selective advantage for the system.

CHAPTER III

A GENERAL SCALING LAW GOVERNING CHEMOTACTIC AND NON-DIRECTED EUKARYOTIC MOTILITY

Introduction: The relationship between directed and non-directed motility.

Cell motility, the movement of cells via intrinsic propulsive mechanisms, plays key roles in health and disease. Two forms, directed and non-directed motility are commonly studied. Directed motility, the best understood example of which is chemotaxis, occurs when the motility of cells is directionally biased as the result of a spatial (or possibly temporal) signal. For example, the homing of neutrophils to sites of infection occurs as the result of the cells ability to sense a gradient of chemokines that are being released by the infected tissue. When experimentally removed from external signals, cells remain motile, yet move in no particular direction, in a non-directed manner.

The two forms of motility are often studied separately, and from different perspectives. Chemotaxis is often studied with the intent of elucidating the signal transduction pathways that allow cells to sense direction in chemoattractant gradients, a process called “directional sensing”. Indeed, directional sensing is remarkable for its sensitivity to weak and noisy chemoattractant concentration gradients [15, 38, 40]. Non-directed motility is often approached from the physical perspective of spontaneous “symmetry breaking” [4]. This is the result of the fact that the cell must choose a direction in which to move despite having no external signal to influence this choice.

Therefore, in the terminology of symmetry breaking, a cell with no polarity and in the absence of a directional cue is in a high symmetry state, in that all directions are equally favorable (i.e., symmetric). As the cell "chooses" a direction from these symmetric possibilities, the cell polarizes and begins to move in that direction, thus "breaking" the symmetry. Once the cell begins to move, its range of motion is restricted and therefore the cell is in a lower state of symmetry.

Despite the apparent differences between non-directed and chemotactic motility, they share many processes at the molecular, subcellular, and cellular level. Most generally, all cell movements require the polymerization of the cytoskeleton. Furthermore, signaling pathways first described to regulate directional sensing downstream of the chemoattractant receptor in *Dictyostelium* were subsequently shown to be spontaneously activated during non-directed motility, in a manner apparently independent of chemoattractant signaling [57]. Both forms of motility share the subcellular processes of protrusion, retraction, and cell polarization, which occur as the result of spatial and temporal coordination of molecular processes. Finally, at the cellular level, displacements of all eukaryotic cells during non-directed motility are not truly random but instead to contain periods of directional persistence in which the cell moves more or less in a straight line. Therefore, the movements of the cells during non-directed motility are often described as a persistent random walk[71]. Conversely, the movements of cells undergoing chemotaxis are not perfectly linear but contain random reorientations and therefore are best described as a biased random walk[38, 67].

Therefore, both forms of motility contain directional persistence and elements of randomness that give rise to reorientations.

As a result of the similarities between the two forms of cell motility, it is desirable to identify an analytical framework applicable to both forms of motility and therefore potentially capable of revealing unifying principles that govern the full range of eukaryotic cell motility, including non-directed and chemotactic. We approached this problem by realizing that, in general, the persistence and randomness present in both forms of motility as well as the transitions between them likely arise from the same underlying mechanisms. This prompted us to apply bimodal analysis which segregates the movements of a cell into alternating persistent and reorientation modes based on the direction in which the cell is traveling. Bimodal analysis is equally applicable to both non-directed motility and chemotaxis and offers several advantages over existing methods of analyzing cell motility, particularly, the estimation of persistence time. First, bimodal analysis is not based on a theoretical model of cell motility. A recent study has cast doubt on many of the assumptions required for the derivation of the persistent random walk model and even suggests that one may be required to derive a model specific to the properties of each individual cell line [72]. Such a conclusion makes a model-free method, such as bimodal analysis, more attractive. Secondly, by treating persistent and reorientation modes independently, bimodal analysis offers a measurement not only of some characteristic time for persistent motility but also for reorientation.

We exploited these advantages to compare the average time spent in directional mode to the average time spent in reorientation mode for wild type *Dictyostelium* cells during both non-directed and chemotactic motility. Despite the fact that the mean reorientation mode time is free to vary independently of mean persistent mode time, we found them to be locked into a non-linear negative correlation. On a log-log scale, the non-linear relationship between the mean mode times is linear, revealing that both forms of motility to be described by a simple scaling law. Furthermore, we identified four perturbations in which the scaling relationship between persistence and reorientation time was significantly altered, providing insight into the mechanisms that give rise to this law. To generalize our findings, we show the same scaling law to describe the non-directed motility of three human cell lines. We propose this scaling law to be the signature of a mechanism that gives rise to the full range of cell motility including non-directed and chemotactic.

Methods.

Cell Culture.

Dictyostelium cells were cultured axenically in HL5 medium supplemented with glucose and antibiotics. For all assays, cells were resuspended from petri dishes and cultured in suspension. For vegetative non-directed motility, the cells were cultured overnight in suspension and then transferred to either a microfluidic channel bonded to a glass substrate (the case for some *wt*, *pi3k1/2*$^{-}$, and *pten*$^{-}$ cells) or a glass-bottomed

dish (for the remaining cells) for time-lapse imaging. For developed non-directed and directed assays, cells were cultured in suspension for three days. 1.5 x 10^8 cells were washed three times and resuspended in 30mL of Na/K phosphate buffer. cAMP was then delivered to the cells every 6 minutes for 5 hours. Mutant *Dictyostelium* cells were obtained from the *Dictyostelium* stock center. The culture of MCF10A cells and HL60 cells is described in [73]and [60], respectively. HT1080 cells were cultured in Dulbecco's Modified Eagle Medium supplemented with 10% FBS.

Cell motility assays and cell tracking.

The imaging of *Dictyostelium* cells and the particulars of the micropipette and microfluidic assays was previously described in [74]. All assays in a microfluidic device used the same flow rate as in [74]. Using a Rayleigh test, there was no evidence that the presence of flow directionally biased the movements of cells (data not shown). For *wt* cells and mutants, developed non-directed and micropipette assays were performed after five hours pulsing with cAMP. The exceptions to this were *gα2*$^-$ and *aca*$^-$ mutants which were allowed to develop for longer periods. For aggregation assays, cells were pulsed for at least five hours, plated, and regularly checked for signs of aggregation. Upon the onset of streaming and aggregation, time-lapse imaging initiated and cells were tracked as they approached the aggregation center. All time-lapse images were obtained every three seconds using 20x DIC objective and Metamorph. All cell displacements were obtained using the "Track Objects" function in Metamorph. Cells

were tracked for a minimum of 10 minutes but were often tracked for up to one hour. Blebbistatin was used at a concentration of 6μM and nocodazole at a concentration of 15μM.

For neutrophils (HL60) Substrates were pre-treated with 100μg/mL fibronectin for one hour. All experiments used 20x DIC optics and were imaged every 5 seconds for at least 20 minutes. Cell centroids were tracked with Metamorph “track objects” function.

The motility assays for MCF10A cells has been previously described in [73]. Briefly, cells were imaged every 0.5 minutes using 40x phase contrast optics. Cell centroids were manually tracked. Fibrosarcoma cells (HT1080) in suspension were plated on culture dishes pre-treated with 2.5μg/mL fibronectin. Images were obtained using a 10x phase contrast objective every 2 minutes. Cell centroids were manually tracked using the ``Measure XYZ distance'' function in Metamorph. Cells were tracked for a period of 4 to 6 hours.

Bimodal Analysis.

Bimodal analysis, which segregates a cell path into alternating persistent and reorientation modes, is fully described in [73]. Briefly, the first step in isolating persistent and reorientation modes requires the determination of the instantaneous direction change, φ, for every time point, t. The values of $\varphi(t)$ are then compared to an empirically defined cut-off angle, φ_{cut}, with time points with values of $\varphi(t) < \varphi_{cut}$ becoming candidates for a persistent mode. A second criterion is then applied, requiring at least three successive time points with $\varphi(t) < \varphi_{cut}$ before defining a persistent mode.

All other movements belong to reorientation modes. In the present work, the value for φ_{cut} was set to 45˚. The reorientation angle, ϑ, is computed as the angle between two successive persistent modes. The overall direction of a persistent mode was determined using a multi-point linear regression of all the data points in that particular mode. See figure S4 for a more complete definition of reorientation angle.

Statistical Analysis.

All statistical analyses were done in Matlab. Correlation coefficients, *r*, and their associated *p*-values were computed using the function "corrcoef.m". Slopes (scaling exponents β) were compared by ANCOVA (function aoctool.m). If significant differences within the entire data-set were detected by ANCOVA (i.e., the p-value of interaction term less than 0.05), pairwise multiple comparisons were then made by a *t* statistic. This statistic was defined as the ratio of the difference of the slopes estimates to the pooled standard error for each estimate (i.e., corrected for different sample sizes for each genotype/cell line). With the exception of *pi3k1/2*$^{-}$, the residuals from all fits were shown to be normally distributed by the Lilliefors test (lillietest.m). Comparisons of the probability distributions of and for different assays were compared using a Kolmogorov-Smirnoff test for two identical distributions (kstest2.m). The dispersion of the turn angle distributions were compared using a custom randomization test.

Simulation of persistent random walk.

Cell migration is most commonly and widely described as a persistent random walk motion [72] which is emergent from the Langevin equation [75, 76]:

$$m\frac{d\vec{v}(t)}{dt} = -\xi\vec{v}(t) + \vec{f}(t), \quad (1)$$

where m is the mass of a single cell, $\vec{v}(t)$ is the cell velocity, ξ is an effective friction coefficient, and $\vec{f}(t)$ is random force acting on the cell. The first term on the right-hand side denotes the friction force which the cell experiences due to the motion in a given medium. The second term denotes the random stochastic force which has two characteristic properties: (i) a mean of zero $\langle \vec{f}(t) \rangle = 0$; and ($ii$) δ-functional correlations, $\langle \vec{f}(t) \cdot \vec{f}(t') \rangle = 2n\xi k_B T\delta(t-t')$ [76], where k_B is the Boltzmann constant, T is the absolute temperature, and n is the dimensionality.

Uhlenbeck and Ornstein [77] showed that mean-squared displacement, $\langle \Delta r(t)^2 \rangle$, can be obtained by integrating the simplified stochastic differential equation (1) to yield:

$$\langle \Delta r(t)^2 \rangle = \frac{2mk_B T}{\xi^2}\left(\frac{\xi}{m}t - 1 + \exp(-\xi t/m)\right). \quad (2)$$

Using the equipartition theorem, $k_B T = m\langle v^2 \rangle$, and redefining m/ξ as P, we obtain a following equation:

$$\langle \Delta r(t)^2 \rangle = 2\langle v^2 \rangle P(t - P + P\exp(-t/P)), \quad (3)$$

where P is the persistence time.

Numerically solving equation (1), we have performed a persistent random walk simulation of a range of persistent times and speed.

Results.

A Scaling Law for *Dictyotselium* motility.

In an effort to understand the subcellular processes that give rise to directional persistence during both non-directed and chemotactic motility in *Dictyostelium*, we examined the dynamic localization of mRFP labeled F-actin-binding domain (LimE-Δ-coil) [78] in wild type (*wt*) cells. Interestingly, during non-directed motility oscillations between two distinct patterns of localization were clearly seen within a single cell. (Fig. 12A). For periods of time, a cell would polymerize actin in brief pulses leading to protrusions at apparently random locations around its cortex. This spatially disorganized polymerization led to multiple competing protrusions and resulted in little net

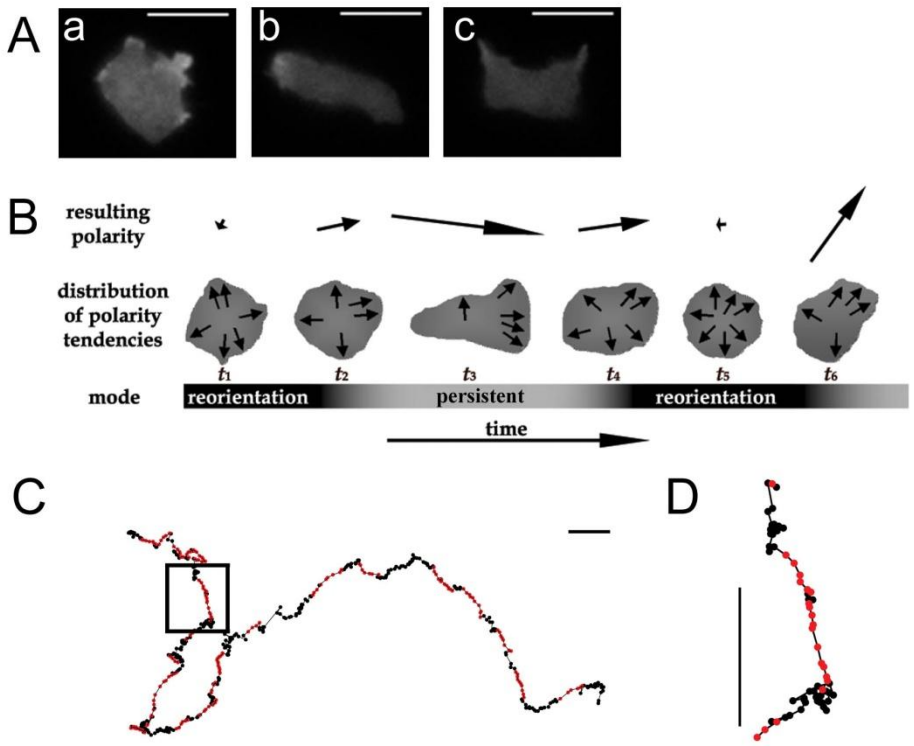

Figure 12. **The application of bimodal analysis to directed and non-directed eukaryotic cell motility**. A) Images of a single *wt* cell expressing mRFP-LimE-Δ-coil. A cell with actin polymerization randomly distributed around its cortex is shown in (a). In (b), a later image of the same cell with organized leading edge and coordinated motility. Eventually, the subcellular organization in (b) is lost, (c). B) A conceptual model for bimodal motility and the application of bimodal analysis to eukaryotic cell motility. During reorientation mode, a cell produces a number of competing tendencies to move in various directions, resulting in uncoordinated motion with little directional persistence. The exit from reorientation mode requires a spontaneous eruption of polarity, resulting in increased directional persistence. The polarity, however, is unstable and eventually the cell returns to reorientation mode. C) An example of bimodal analysis to a *wt Dictyostelium* cell during non-directed migration with a three second sampling interval over 26 minutes. Black points represent reorientation modes while red points represent persistent modes. D) The boxed region of (C), showing in detail the classification into persistent and reorientations modes. All scale bars are 10μms.

translocation of the cell (Fig. 12A(a)). Occasionally, polymerization would occur within one region of the cell, allowing for the accumulation of polarity and persistent motility

(Fig. 12A(b)). Over time, the polarity and the persistent motility dissipated and the cell returned to its more disorganized state (Fig. 12A(c)). Similar oscillations, although less pronounced, were seen during chemotaxis as well.

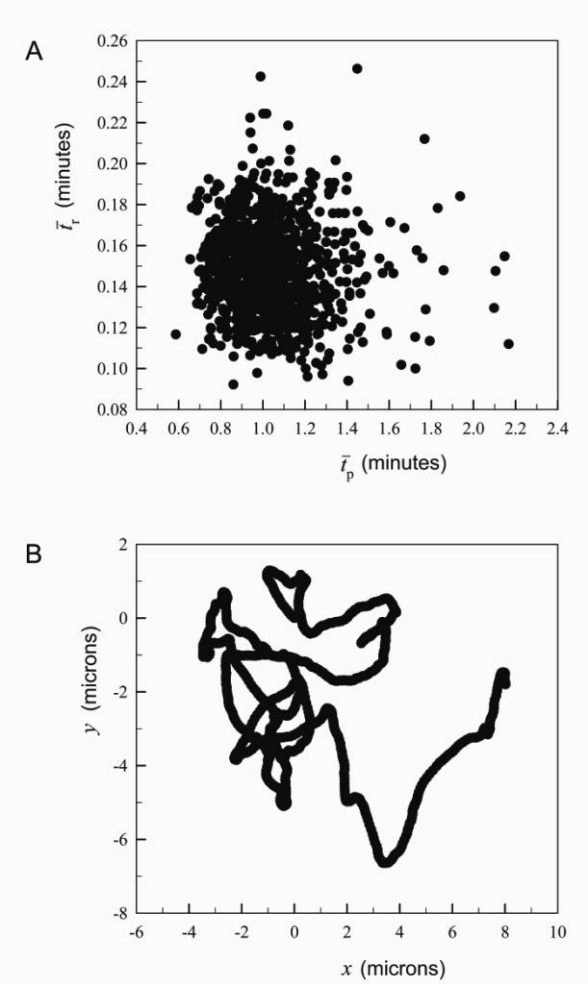

Figure 13. **An example of a non-scaling relationship between mode times in simulated persistent random walk.** A) $\overline{t}_p$ and $\overline{t}_r$ for 1000 simulated persistent random walks. Notice no particular relationship between mean mode times. B) A characteristic trajectory of a simulated persistent random walk. See methods for simulation details.

Table 2. The *Dictyostelium* cell lines, pharmacological treatments, and motility assays along with sample sizes indicated in each case.

Non-directed motility

Cell Line	Vegetative	Developed	12.5 nM cAMP	125 nM cAMP
wt	37	141	35	51
aca^{-}	15	6	-	-
erk^{-}	20	5	-	-
gα2^{-}	14	14	-	-
gca/sga^{-}	9	7	-	-
gsk3^{-}	12	10	-	-
ins6pk^{-}	9	17	-	-
pi3k1/2^{-}	50	38	29	21
pkacat^{-}	12	8	-	-
pldA/C^{-}	9	7	-	-
pldB^{-}	16	21	-	-
pten^{-}	59	43	31	25
wt + BLEBB	12	10	-	-
wt + nocodazole	15	22	-	-
racC^{-}	24	7	-	-
scar^{-}	12	15	-	-
vasp^{-}	11	25	-	-
wasp^{TK}	16	10	-	-

Chemotaxis

Cell Line	pipette	microfluidic	aggregation
wt	107	61	14
aca^{-}	19	-	-
erk^{-}	9	-	-
gα2^{-}	11	-	-
gca/sga^{-}	16	-	5
gsk3^{-}	12	-	-
ins6pk^{-}	15	-	-
pi3k1/2^{-}	121	27	-
pkacat^{-}	6	-	-
pldB^{-}	11	-	-
pten^{-}	51	40	-
wt + BLEBB	16	-	-
wt + nocodazole	17	-	-
racC^{-}	23	-	-
scar^{-}	11	-	-
vasp^{-}	24	-	-
wasp^{TK}	9	-	-

These observations led to a conceptual model of motility as repeated symmetry breaking, i.e., a repeated transition between a reorientation mode with spatially disorganized protrusions (high symmetry), and persistent mode associated with cell polarity and efficient motility with more polarity (low symmetry) (Fig. 12B). The presence of two apparent motility modes prompted us to apply bimodal analysis [73] to classify the displacements of individual *wt Dictyostelium* cells as belonging to either a directionally persistent or a reorientation mode. An example of the analysis on non-directed motility of a *wt* cell is shown Fig. 12B and C. So that we could look for general principles potentially underlying the wide range of motility available to *Dictyostelium*, we analyzed data from both non-directed and chemotactic motility (See Table 2 for assays and sample sizes).

In contrast to the estimation of persistence time[79], bimodal analysis treats persistent and reorientation modes as separate processes, and therefore provides independent measurements of the mean time spent in both persistent mode, $\bar{t}_p$, and in reorientation mode, $\bar{t}_r$. Despite the fact that $\bar{t}_p$ and $\bar{t}_r$ are free to vary independently (Fig. 13), we found a strong inverse relationship between them (Fig. 14A). The relationship between $\bar{t}_p$ and $\bar{t}_r$ has an immediate biological consequence: it suggests the subcellular processes that govern the eruption and the dissipation of persistent mode to be coupled, for an increase in $\bar{t}_p$ requires the reduction in $\bar{t}_r$. A log-log plot linearizes the data, revealing a scaling relationship such as is commonly seen in complex systems near critical points [80]. The inverse scaling relationship seen here for cells

directly contrasts with the positive scaling relationship between search and motion phases (akin to our reorientation and persistent modes, respectively) in animal foraging [81]. Remarkably, this representation allows for an elegantly simple description of the data from both non-directed motility and chemotaxis by a single scaling exponent of β=-1.11 (Fig. 14A, inset).

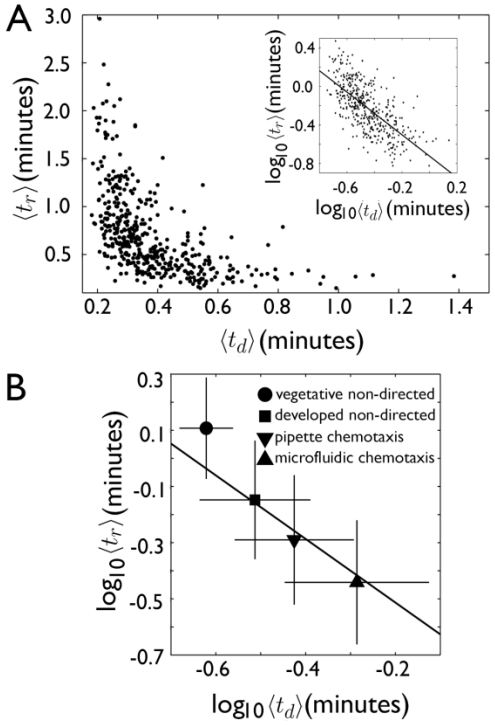

Figure 14. **A scaling law between mean mode times.** A) A nonlinear relationship exists between mean persistent time, $\overline{t}_p$, versus mean reorientation time, $\overline{t}_r$, from 446 *wt Dictyostelium* cells from six different motility assays. *Inset,* A log-log plot linearized the data and allows for the estimation of the scaling exponent β= -1.11. B) The scaling law describes the full range of *Dictyostelium* motility, including directed and non-directed motility

Table 3. **The statistical analysis of scaling in individual assays for *Dictyostelium* cells. *r* and *p*-values are the correlation coefficients between $\log \bar{t}_p$ and $\log \bar{t}_r$ for each genotype and its associated probability.**

Assay	Slope (*β*)	*r*	*p*- value	*n*
Vegetative	-1.6529	-0.5401	0.0006	37
Developed	-0.8914	-0.5187	4.44×10^{-11}	141
Pipette	-0.8717	-0.4682	3.68×10^{-7}	107
Microfluidic	-0.8434	-0.6136	1.46×10^{-7}	61

The curve shown in Fig. 14A provides a unifying description of the full range of directional persistence of *Dictyostelium* cells, including both chemotaxis and non-directed motility. In Fig. 14B, the mean mode times for non-directed vegetative, non-directed developed, and chemotaxing *wt* cells in a micropipette assay and in a microfluidic device are shown. Developed *Dictyostelium* cells are known, on average, to move faster and with greater coordination than vegetative cells [82]. Likewise, developed cells are known to move faster when undergoing chemotaxis as compared to non-directed motility. Additionally, we recently showed that *wt* cells performed chemotaxis with greater efficiency in the microfluidic device compared to the micropipette assay [74]. Consistent with these expectations, as the coordination of the motility is increased from vegetative non-directed motility to chemotaxis, the position of the cells on the curve "slides" to the right, indicating increased persistent time and decreased reorientation time.

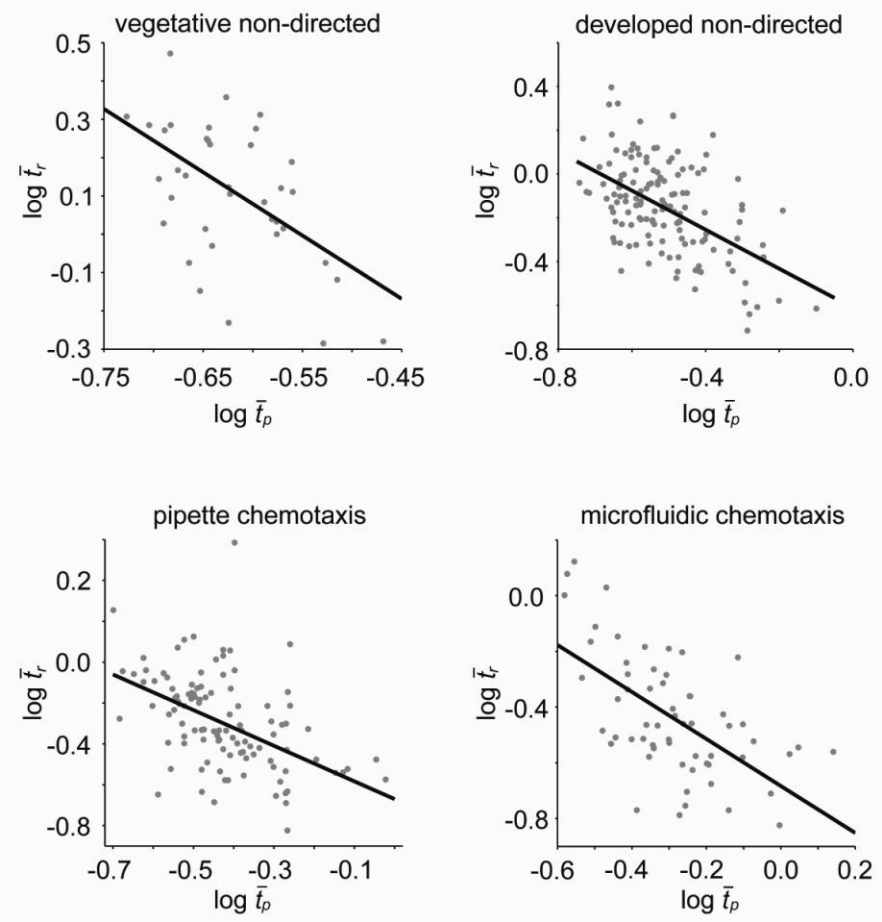

Figure 15. **The scaling between t_p and t_r describes cell-to-cell variability in vegetative non-directed, developed non-directed, developed pipette chemotaxis, and developed microfluidic chemotaxis.**

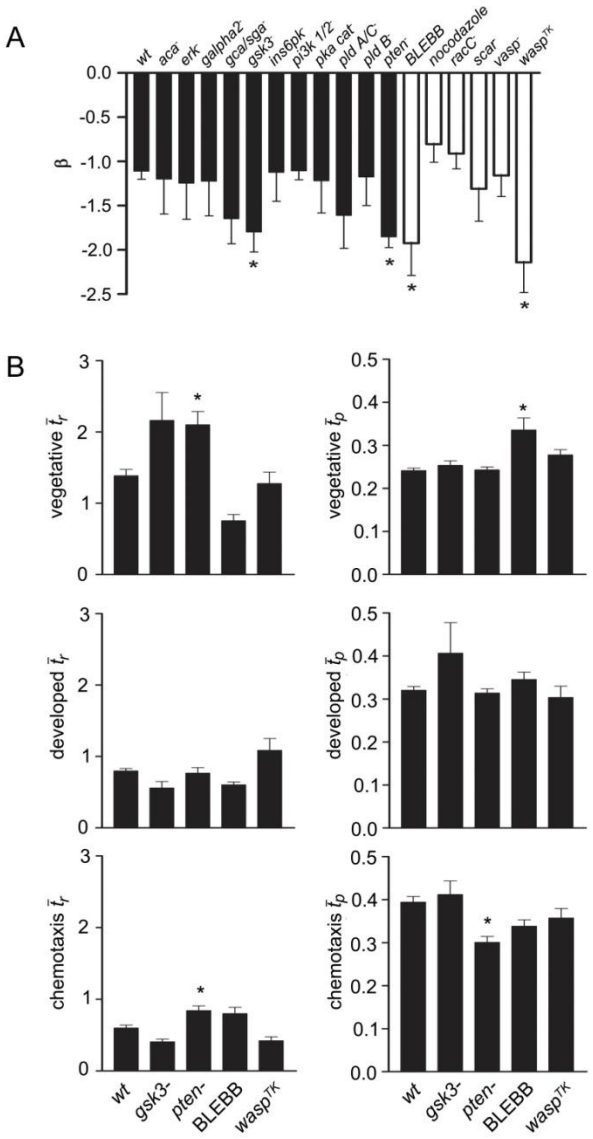

Figure 16. **Analysis of scaling in mutants.** A) The values of the scaling exponent β plus the standard error of the estimates for all perturbations. Perturbations are grouped by signal transduction (black bars) and cytoskeletal regulators (white bars). See Table 4 for details. B) Comparison of $\overline{t}_p$ and $\overline{t}_r$ for the four mutants in vegetative non-directed (top), developed non-directed (middle), and developed chemotaxis (bottom). For both A and B, the star indicates statistical difference from *wt* at the $p < 0.05$ level.

Table 4. **The statistical analysis of the scaling relationships between t_p and t_r for individual *Dictyostelium* cell lines and pharmacological treatments**. *r* and *p*-values are the correlation coefficients between $\log \bar{t}_p$ and $\log \bar{t}_r$ for each genotype and its associated probability. The comparison *p*-value is the pairwise comparisons of slopes estimated by ANCOVA for each perturbation compared to the estimate for *wt*. The slope comparisons were performed via a two-tailed test. Therefore, for significance at the $p < 0.05$ level, only values $0.025 < p < 0.975$ were considered significant.

cell line	*β*	*r*	Correlation *p*-value	Comparison *p*-value	*N*
wt	-1.1087	-0.6748	1.47×10^{-60}	-	446
aca$^-$	-1.1984	-0.5107	7.59×10^{-4}	0.5897	40
erk$^-$	-1.2452	-0.457	0.0066	0.6295	34
gα2$^-$	-1.2228	-0.5274	0.0006	0.6143	39
gca/sga$^-$	-1.6475	-0.7878	7.17×10^{-9}	0.9725	37
gsk3$^-$	-1.796	-0.7142	2.1×10^{-6}	0.9982	34
ins6pk$^-$	-1.121	-0.4541	0.0029	0.5146	41
pi3k1/2$^-$	-1.1045	-0.6180	1.6×10^{-31}	0.4828	286
pkacat$^-$	-1.2183	-0.6555	2.74×10^{-4}	0.6182	26
pldA/C$^-$	-1.6086	-0.8002	0.0002	0.9085	16
pldB$^-$	-1.1737	-0.5259	0.0001	0.5794	48
pten$^-$	-1.8515	-0.7347	1.64×10^{-43}	0.9999	249
wt + BLEBB	-1.9238	-0.7673	1.91×10^{-8}	0.9879	38

wt + nocodazole	-0.8059	-0.4851	0.0002	0.067	54
racC^{-}	-0.9122	-0.5893	2.7 x 10^{-6}	0.1235	54
scar^{-}	-1.3093	-0.5989	0.0001	0.7090	38
vasp^{-}	-1.159	-0.4587	0.0002	0.5811	60
wasp^{TK}	-2.1401	-0.7537	1.72 x 10^{-7}	0.9986	35

As all aspects of non-directed motility arise from intrinsic cell processes, the observation of a scaling relationship during non-directed motility reveals the mechanism relating $\bar{t}_p$ to $\bar{t}_r$ to be an intrinsic property of the cell. When considered separately, the presence of the same scaling law in each assay (Fig. 15 and Table 3), even in non-directed motility, indicates that cell-to-cell variability is also described by this law. Exactly what subcellular processes are varied from cell-to-cell or from vegetative to developed cells during non-directed motility is not clear. However, the fact that cells undergoing chemotaxis also fall on this scaling curve (Figure 13B) suggests that chemoattractant-driven signal transduction harnesses these intrinsic processes (and its cell-to-cell variability) while tuning their specific properties, to increase directional persistence and reduce reorientations.

If a particular molecular pathway is responsible for coupling $\bar{t}_p$ to $\bar{t}_r$, genetic or pharmacological perturbation of that pathway might be expected to eliminate

directional persistence, and therefore $\bar{t}_p$, during non-directed motility. Additionally, a perturbation might sever the tuning of the coupling of $\bar{t}_p$ and $\bar{t}_r$, and thereby eliminate or alter the scaling relationship. To address the effect of perturbations on the mechanism relating $\bar{t}_p$ to $\bar{t}_r$ we examined the relationship between $\bar{t}_p$ and $\bar{t}_r$ for a total 17 genetic mutants or cells treated with pharmacological inhibitors in vegetative non-directed, developed non-directed, and the pipette chemotaxis assay. We chose cells lacking signal transduction molecules reported to be important for chemotaxis and established cytoskeletal regulators (Fig. 16 and Table 2 for a list and sample sizes). We were unable to eliminate directional persistence, suggesting the cycling between persistent and reorientation modes to be a robust property of the cell. Furthermore, all perturbations retained a significant scaling relationship between $\bar{t}_p$ and $\bar{t}_r$ (see Fig. 16A and Table 4). However, four perturbations, loss of GSK3, PTEN, or WASP and inhibition of myosin II, resulted in statistically different values for β (Fig. 16A). We note that each of these perturbations has been reported to reduce the cytoskeletal and morphological polarity thought to be important for efficient, coordinated motility [27, 83-85].

The scaling exponent β describes the behaviour of the cells in three separate motility assays, vegetative non-directed, developed non-directed, and developed chemotaxis. We examined the behaviour of the four mutants that are different from *wt* in more detail in an attempt to isolate the defect to a single motility assay (e.g., vegetative non-directed motility). To do this, we compared the mean mode time for each perturbation in each assay to *wt* (Fig. 16B). *pten*$^-$ cells had a higher $\bar{t}_r$ during

vegetative non-directed motility, while, during chemotaxis, both a lower $\overline{t}_p$ and higher $\overline{t}_r$ contributed to a steeper scaling relationship compared to *wt*. However, removal of either *pten-* vegetative non-directed or chemotaxis failed to return the scaling exponent of *pten-* cells to the value of *wt* (not shown). BLEBB treated cells during vegetative non-directed motility had a higher $\overline{t}_p$ compared to *wt*, suggesting that high levels of myosin II activity contributes to the lack of polarity seen in vegetative cells. Furthermore, the removal of vegetative BLEBB treated cells from the statistical comparison of scaling exponents brought the scaling exponent of BLEBB treated cells up to the level of *wt.* When compared in this fashion, $\overline{t}_p$ and $\overline{t}_r$ for both *gsk3-* and *wasp*^{TK} cells were not different from *wt* in any single assay. Thus more detailed experiments will be required to identify the source of the difference in the coupling of $\overline{t}_p$ and $\overline{t}_r$ in these perturbations.

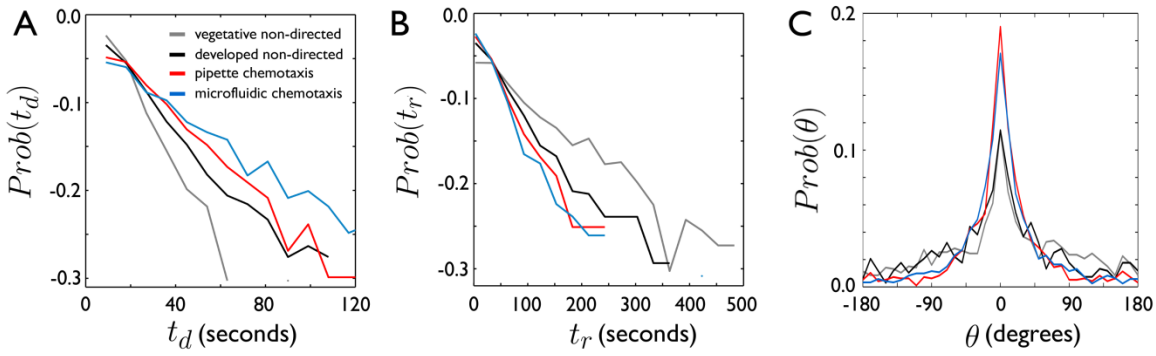

Figure 17. **The probability distributions of persistent time and reorientation angles reveals similarities and differences between directed and non-directed motility.** The probability distributions of $\overline{t}_p$, $\overline{t}_r$, θ and reveals similarities and differences between directed and non-directed motility. A,B) The probability distribution of the duration of $\overline{t}_p$ and $\overline{t}_r$ respectively, for the vegetative non-directed, developed non-directed, developed pipette chemotaxis, and

developed chemotaxis in a microfluidic device of *wt Dictyostelium* cells. C) Reorientation-angle distributions for the assays in (A) reveal increased directional correlation between successive persistent modes during directed motility.

Chemotaxis quantitatively, but not qualitatively, differs from non-directed motility.

The fact that both non-directed and chemotactic motility can be described by the same quantitative law suggests that chemotactic gradients serve to quantitatively tune the inherent cycling between the persistent and reorientation mode. The probability distribution of persistent time is shown in Fig. 17 for *wt Dictyostelium* cells during the four assays described above. Although they differ statistically with chemotaxing cells having larger t_d, overall, the distributions are qualitatively similar in that small values are common with larger values increasingly uncommon. The duration of reorientation time is similarly distributed, though the general trend between assays is reversed (Fig. 17). The qualitative similarity of the mode time probability distributions for both directed and non-directed motility provides further evidence that the presence of a directionally biasing gradient (e.g., chemoattractant gradient) merely quantitatively tunes the mechanism that governs the transition from t_p to t_r and back, rather than qualitatively altering its overall nature.

The most striking difference between non-directed and chemotactic motility is revealed by considering the reorientation angle distribution, or the distribution of the

angles, θ, between successive persistent modes (Fig. S4) of *wt Dictyostelium* as illustrated in Fig. 4B. During vegetative and developed non-directed motility, the turn-

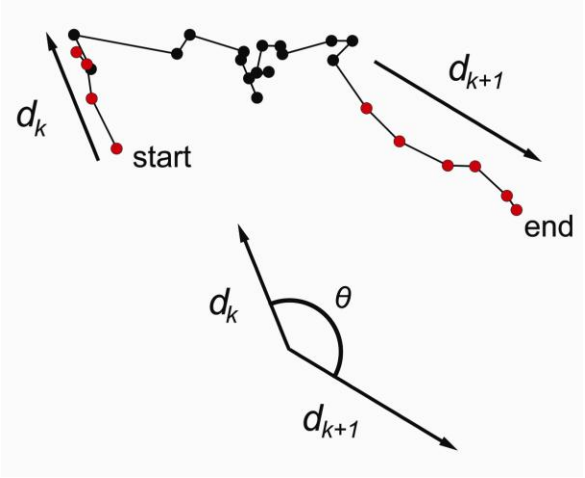

Figure 18. **The definition of reorientation angle.** A portion of a cell's path is shown. The cell begins at "start" in a persistent mode, labelled d_k (red circles). The overall direction of d_k is shown by the corresponding arrow. The cell then enters into a reorientation mode, depicted with black circles. Eventually, the cell leaves reorientation mode and enters into a new persistent mode, d_{k+1}. The reorientation angle is defined as the angle between two successive directional modes.

angle distributions are broadly distributed yet peaked around 0˚, indicating that even during non-directed motility, eukaryotic cell motility has a degree of directional persistence. This is expected given that, due to the time scale of the cytoskeletal rearrangements required for cellular propulsion, wide-angle reorientations should be rare compared to small angle reorientations. According to our model (Fig. 12B), the transition from reorientation mode to persistent mode requires the development of a comparatively ordered, subcellular polarization from a disordered state. One prediction

of our model is that the longer a cell spends in a directionally randomizing reorientation mode and the longer it takes to polarize, the larger the turn angle would tend to be. Accordingly, we found that the wide turn angles were indeed associated with longer reorientations, especially for non-directed motility (Fig. 19). The reorientation angle distribution for chemotactic *wt* cells, in contrast, is less broadly dispersed despite having statistically identical mean values. Chemotactic gradients, therefore, result in the cell spending more time in persistent mode and a higher directional persistence lasting throughout intervening reorientation modes.

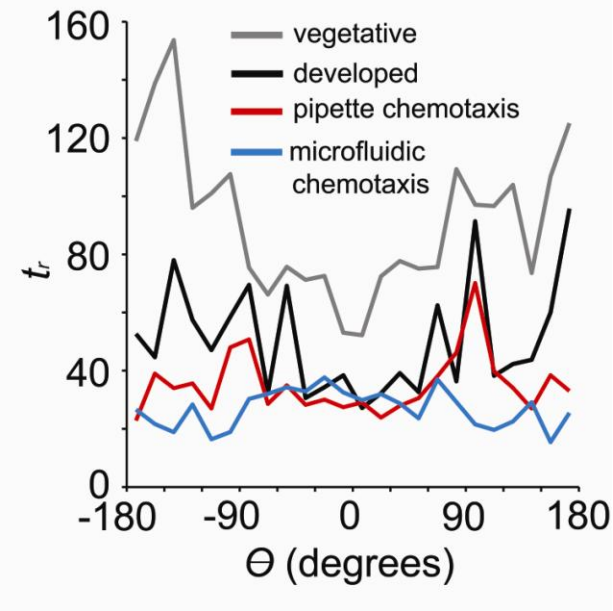

Figure 19. **Mean reorientation time, t_r, as a function of reorientation angle, θ.** Note that longer reorientation times tend to correspond to larger reorientation angles, especially for both forms of non-directed motility.

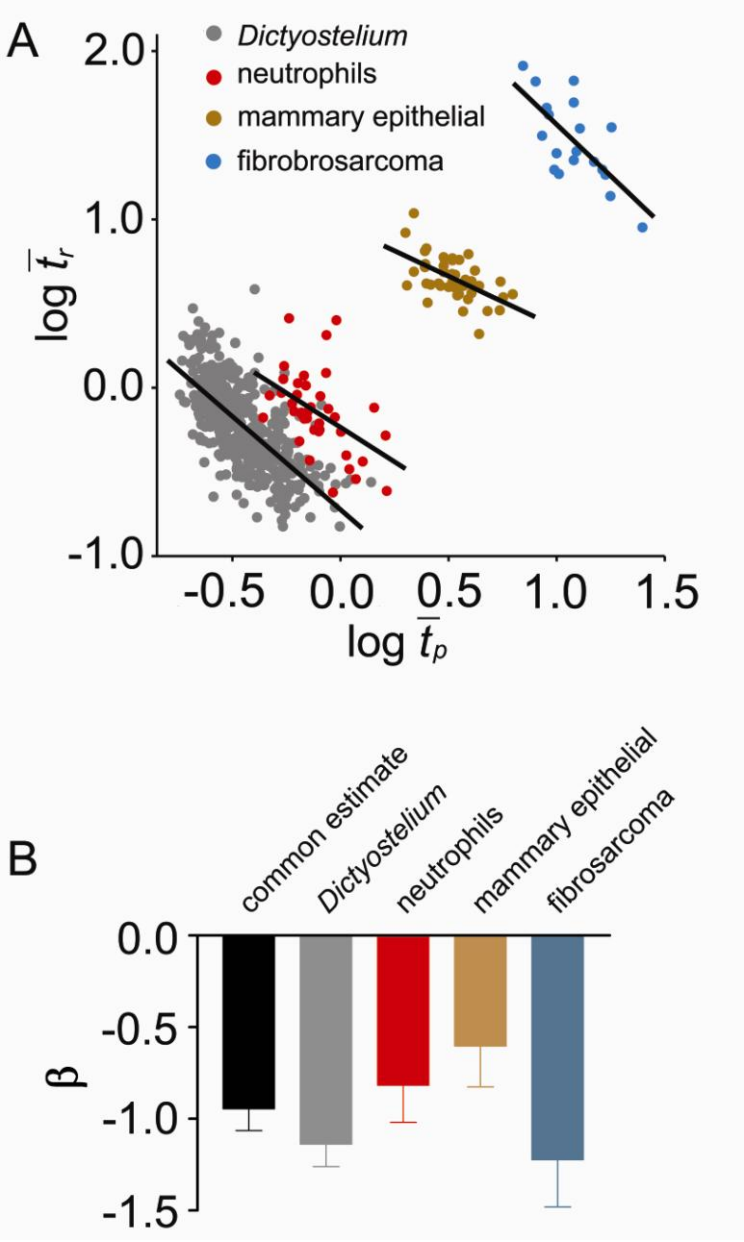

Figure 20. **The generalization of the scaling mechanism to human cells.** A) Comparison of *Dictyostelium* cells, human neutrophils, mammary epithelial, and fibrosarcoma cells. B) ANCOVA

analysis of the scaling exponents for each cell line. The scaling exponents for each cell line were not statistically different allowing for the estimation of a common scaling exponent of β= -0.938.

Table 5. **Scaling relationships for t_p and t_r between *wt Dictyostelium* and human cell lines.** *r* and *p*-values are the correlation coefficients between $\log \bar{t}_p$ and $\log \bar{t}_r$ for each genotype and its associated probability. ANCOVA revealed no significant differences in values of β for the cell lines, *p*=0.1202.

Cell Line	Slope (β)	*r*	Correlation *p*-value	*n*
Dictyostelium	-1.1087	-0.6609	3.13×10^{-167}	446
Neutrophils (HL60)	-0.8174	-0.464	0.0029	39
Mammary epithelial (MCF10A)	-0.6037	-0.5554	0.0001	42
Fibrosarcoma (HT1080)	-1.2226	-0.6962	0.0009	19

Generalization to human cancer cells.

Given the apparent generality of the mechanism relating $\bar{t}_p$ and $\bar{t}_r$ in *Dictyostelium*, we applied bimodal analysis to three motile human cell lines undergoing non-directed motility, neutrophils (*n*=39), mammary epithelial cells (*n*=42) expressing two mutant forms of the Her2 oncogene[73], and fibrosarcoma cells (*n*=19). Not surprisingly, these cell lines possessed different mean mode times (Fig. 20), presumably reflecting the diversity of the time scales inherent in the molecular and subcellular processes

underlying motility for each cell line. All three cell lines produced significant scaling relationships with exponents similar to *Dictyostelium* (Fig. 20B and Table 5). Statistical comparison of the scaling exponents revealed no significant differences between the human cell lines and *Dictyostelium* allowing for the estimation of a common scaling exponent for all cell lines of β=-0.94. The presence of an identical scaling exponent in these diverse cell lines indicates the work of a very general mechanism, operating at different time scales, to relate t_p to t_r in eukaryotic cells.

The effect of bimodal motility on cell speed.

The possession of long persistent time was proposed to increase the search efficiency of *Dictyostelium* non-directed motility [71], while efficient chemotaxis, by nature also requires long persistence times. The ratio of $\overline{t}_p$ to $\overline{t}_r$, revealing the excess of time spent in persistent mode, then, might serve as for a measure of motility efficiency. Indeed the ratio of $\overline{t}_p$ to $\overline{t}_r$ is a strong statistical predictor of mean cell speed for fast moving *Dictyostelium* (r=0.85, p=1.28 x 10^{-122}) and neutrophils (r=0.64, p=1.30 x 10^{-5}), further supporting this suggestion (Fig. 21A). However, the ratio failed to be a significant predictor of mean speed for both slow moving mammary epithelial cells (r= -0.20, p=0.21) and fibrosarcoma cells (r=0.4322, p=0.065) suggesting that speed in these cells is regulated in a different manner from *Dictyostelium* and neutrophils.

Mean speed in either persistent mode $(\overline{s}_p)$ or reorientation mode $(\overline{s}_r)$ also correlated strongly with mean cell speed for all cells. Interestingly, for *Dictyostelium,*

neutrophils and fibrosarcoma cells, $\overline{s}_p$ was found to be significantly greater than $\overline{s}_r$ ($p<10^{-308}$, $p=1.1 \times 10^{-23}$, and $p=0.012$, respectively) indicating that higher speeds, were associated with persistent mode (Fig. 21B). This is consistent with a saltatory model of non-directed motility in vegetative cells suggested in [86], and our model of coordinated cytoskeletal dynamics in persistent mode (Fig. 12B). Interestingly, for the mammary epithelial cells, there was no difference between mode speeds ($p=0.92$). It has been proposed that the subcellular processes that drive the motility of faster cells like neutrophils and *Dictyostelium* to be farther from equilibrium than the related processes in slower moving cells [86]. We propose the variation in speed between persistent and reorientation mode for *Dictyostelium* and neutrophils, as compared to mammary epithelial and fibrosarcoma cells, to similarly reflect the distance from equilibrium in the cytoskeletal processes that regulate cell speed.

Given that the speed of *Dictyostelium*, neutrophils, and fibrosarcoma cells is higher in persistent mode than in reorientation, it is important to examine the relationship between speed in reorientation and speed persistent modes. We found that there was a strong correlation between $\overline{s}_p$ and $\overline{s}_r$ for cells examined here (Fig. 21, and Table 6). In fact, all the cells studied here that were relatively fast in reorientation mode were also fast in persistent mode. As a result, the overall mean speed of the cell appears to be largely set by factors extrinsic to the regulation of persistent and reorientation modes despite the fact that speed can vary between modes.

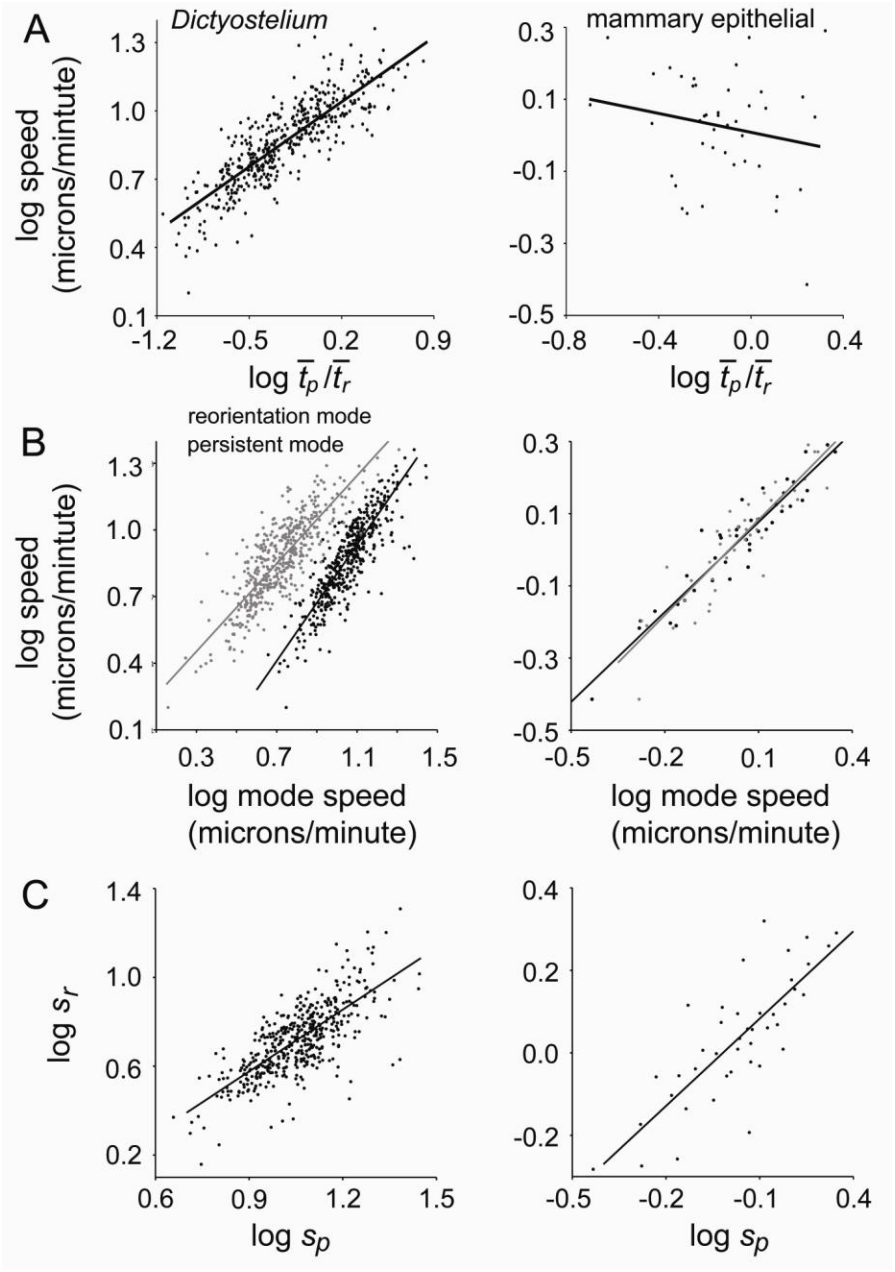

Figure 21**. The effect of bimodal motility on cell speed.** A) The ratio of $\overline{t}_p$ to $\overline{t}_r$ is a strong predictor of mean cell speed for *Dictyostelium* (left) but not mammary epithelial cells (right). B) Mean mode speeds correlate with mean speed for both (left) *Dictyostelium* and mammary epithelial cells (right). For *Dictyostelium* cells, however, the mean speed in persistent mode is significantly higher than the mean speed in reorientation mode. Thus for fast moving cells, the regulation of persistent and reorientation mode effects mean speed. C) A correlation between mean speed in reorientation mode and mean speed in persistent mode suggests that speed is largely controlled by factors extrinsic to the regulation of bimodal motility.

Table 6. **Correlations between mean mode speeds for all four cell lines studied.**

Cell Line	*r*	Correlation *p*-value
Dictyostelium	0.75	6.7×10^{-288}
Neutrophils (HL60)	0.93	1.4×10^{-17}
Mammary epithelial (MCF10A)	0.80	2.0×10^{-10}
Fibrosarcoma (HT1080)	0.64	0.0035

Discussion.

Our understanding of the detailed mechanisms that regulate particular aspects of cell motility has rapidly expanded in recent years. New molecules have been identified and model systems have become increasingly diverse. With this increase in detail and diversity comes a new challenge: to integrate the findings from these diverse systems into a unified framework. Our results provide a simple, unified description of both directed and non-directed eukaryotic cell motility. Previous attempts to unify our understanding of both directed and non-directed motility were based on the concept of receptor noise [79]. However, this effort did not consider non-directed motility in the absence of chemoattractant. Further, it has been shown that non-directed motility can take place in the absence of conventional constitutive receptor activation [57],

indicating the presence of other mechanisms leading to spontaneous symmetry breaking.

Scaling laws are often seen in complex systems near equilibrium phase transitions and also in self-organizing, non-equilibrium systems tuned near their critical points[80]. The dynamics of the actin-myosin cytoskeleton have been shown to possess hallmarks of complex, self-organizing systems: scaling of mechanical behaviours[87, 88], spontaneous symmetry breaking [4, 89, 90], and travelling waves of actin polymerization and membrane protrusion [78, 82, 91-93]. The identification of scaling behaviour in a system provides significant motivation for the development of quantitative theories that start with system dynamics, attempting to explain the higher-order scaling behaviour in a mechanistic fashion. The presence of a scaling law governing directional persistence and reorientation in four eukaryotic cell lines, from different phyla and tissues and each with different motility characteristics, suggests the existence of a general mechanism regulating the directional persistence (or lack therefore) in eukaryotic cell motility. It remains a significant challenge to understand the dynamic molecular processes that give rise to this scaling relationship.

Regardless of the ultimate origin of the scaling law shown here, our ability to describe, for the first time, the entire range of *Dictyostelium* motility by a single scaling exponent reveals a deep connection between non-directed motility and chemotaxis. We hypothesize that the transition from non-directed motility to chemotaxis occurs through the tuning, via chemoattractant-induced signalling, of the subcellular processes

responsible for the stability of, or the transition between, persistent and reorientation modes. Our identification of four perturbations that quantitatively modify the scaling relationship provides a window into the molecular mechanism(s) that give rise to the coupling of persistent and reorientation modes.

Dictyostelium cells are capable of detecting extremely weak gradients of chemoattractant. It has been shown that they can sense gradients in the nM range [15] with an estimated difference in receptor occupancy from anterior to posterior in the range of 130 receptors [40]. Based on the assumption that the directional persistence in chemotaxis results from instructions to the cytoskeleton from signal transduction, analyses of the sensory processes concluded that chemotaxis occurs near the limit set by noise [38, 40]. However, feedback from the cytoskeleton to the sensory apparatus has been suggested [24]. Although chemoattractant signalling undoubtedly biases the direction of motility, our results suggest that the directional *persistence* during chemotaxis to be intimately related to intrinsic directional persistence during non-directed motility. Combining this notion with the observation that cells can break symmetry and move with directional persistence without receptor signalling [57], it seems that a deep understanding of chemotaxis will require knowledge of the interrelationship between the extrinsically driven signal transduction pathways and intrinsic cellular processes. Therefore, it is likely that a comprehensive understanding of the mechanisms giving rise to symmetry breaking and directional persistence during non-directed motility would likewise provide considerable insight into the more physiologically relevant forms of directed motility such as chemotaxis.

CHAPTER IV

PUTTING IT ALL TOGETHER

On the origin of the scaling law.

To date, the mechanism underlying the scaling law governing cell motility is unknown. Two, non-mutually exclusive sources will be covered here. First, we review essential concepts of self-organization and spontaneous cell polarity. Second, a number of recent studies have begun to study the frequency and lifetime of pseudopod protrusion, which, surprisingly, turn out to follow rather simple, reproducible dynamics. As pseudopod protrusion is a key element in amoeboid movement, it seems likely that pseudopod dynamics might be in part responsible for the scaling law relating persistence time and reorientation time. Armed with these ideas, we then combine our findings with the literature to present a novel, integrated view of chemotaxis.

Self-organizing systems.

The concept of self-organization and self-assembly play an important role in numerous areas of biology [94]. Self-assembly defines the organization of numerous individual particles into an equilibrium structure of defined size. A clear example is the

formation of the virus capsoid from its component proteins. Self-organization, on the other hand, involves the formation of transient structures in systems that are far from equilibrium. Most generally, self-organization describes the tendency of some systems to increase in spatial or temporal complexity in the absence of external driving forces. Diverse self-organizing systems share many features including numerous interactions between a large number of similar objects and interplay between positive and negative feedback that regulate the interactions. A key distinction in self-organizing systems is between local and global behavior. Critically, each particle is typically under a few, simple rules that act locally over short spatial and temporal scales. Despite the fact that these rules only act locally, the population as a whole displays complex behavior at scales much larger than the rules governing the system. Importantly, scaling laws frequently appear in study of self-organizing systems.

Spontaneous symmetry breaking.

The concept of symmetry places a great role in physics and many self-organizing systems can be described in terms of symmetry breaking. Symmetry breaking is simply the transitioning of a system with a high number of possibilities into a system with a lower number. To fix the concept of spontaneous symmetry breaking, consider the classic example of a pencil balanced on its tip on a smooth and uniform surface (Fig. 22). When perfectly balanced, the system is in a high symmetry state because it is free to fall in any direction. It is clear that this state is also unstable because, from experience, we

expect the pencil to fall. From casual observation, however, it would be difficult to predict the direction in which it will ultimately fall. But fall it must and it is the microscopic properties of the pencil and surface, where imperfection in the tip or small vibrations exist that determine the direction in which the pencil will topple. The falling of the pencil results in a collapse of the symmetry of the system, leading to the terminology of symmetry breaking.

In the context of non-directed motility, spontaneous symmetry breaking refers to the eruption of polarity by a cell that lacks any spatial influence as is the case in non-directed motility. Although it is free to polarize and move in any direction (a state of high symmetry), spontaneous polarization is the result of the cell "choosing" a single direction out of the many possibilities. The existence of polarity then allows for persistent movement. But the question arises, "How does a cell, whose components are uniformly distributed, "choose" a direction in which to polarize?"

A mechanism for spontaneous formation of cell polarity.

The leading hypothesis is that spontaneous polarity occurs via the amplification of stochastic fluctuations by positive feedback (Fig. 23). In this scenario, due to the randomness inherent in the intracellular environment, local concentrations of key molecules will fluctuate around their mean. When the local concentration occasionally crosses a threshold, they enter into a positive feedback loop, recruiting/activating more

and more until polarity is formed. Thus it is the interplay between random fluctuations and positive feedback that leads to spontaneous symmetry breaking.

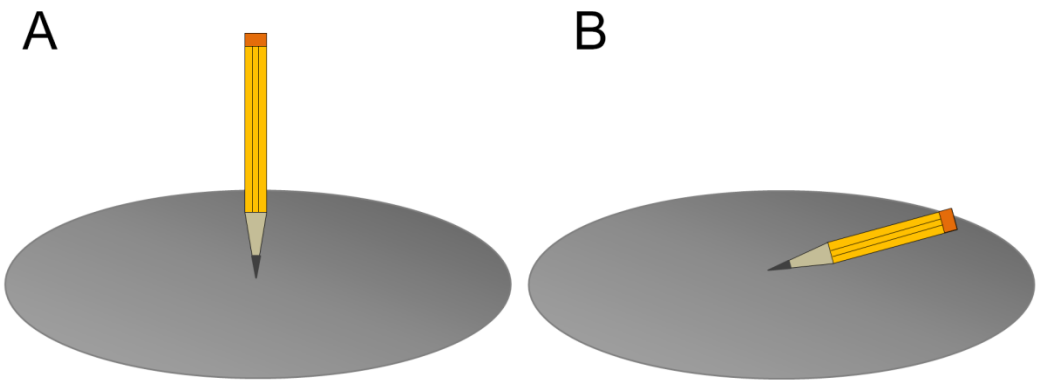

Figure 22. **A cartoon demonstration of symmetry breaking.** A) The pencil is balanced and in a high symmetry state in that it is free to fall in any direction. B) The pencil has fallen and the original symmetry is destroyed, or broken.

Perhaps a few concrete examples will clarify these abstract concepts. The most established example of spontaneous symmetry breaking occurs in the budding yeast. Typically, the bud site forms at locations dictated by landmark proteins which are deposited on the membrane during the previous cytokinesis cycle. However, in mutants lacking functional landmark proteins, bud sites are chosen at random. Li and colleagues examined the examined this processes in detail with live cell fluorescent microscopy [95]. They found that the small GTPase Cdc42 was initially evenly distributed throughout the cell. Over time, puncta formed and eventually a dominant puncta overwhelmed the others and polarity was formed. This process appeared to be independent of any

preexisting structural or chemical polarity. Looking for feedback loops that might drive the spontaneous symmetry breaking, they found that actin and myosin V- based secretory vesicle transport was required for spontaneous Cdc42 membrane localization.

The formation of spontaneous polarity has also been studied extensively in neutrophils [49, 93, 96, 97]. In these studies, Bourne and coworkers first indentified a set of molecules that were exclusive in their localization to either the front of back of a polarized neutrophil. Among those localized to the front included PIP3, Rac, and F-actin, while Rho, Rho Kinase, and myosin. The production of PIP3 at the leading edge was shown to depend on a positive feedback loop involving Rac and F-actin. They proposed front signals to be incompatible with back signals. Coupling this mutual incompatibility with positive feedback led to the spontaneous polarization. Subsequently, others have shown the spontaneous activation of PI3K (and thus the production of PIP3) to be critically dependent on polymerized actin [98].

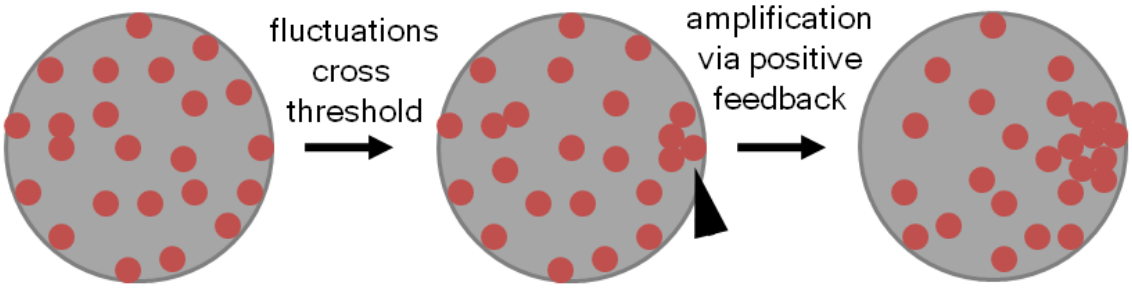

Figure 23. **Spontaneous polarity through amplification of fluctuations.** Initially, components are uniformly distributed (left). Due to thermally driven fluctuations, regions of the cell will become

locally enriched (arrowhead, center). The locally restricted increased density will become amplified due to positive feedback.

Thus, in these two examples of spontaneous polarization, it appears that positive feedback coupled to the F-actin cytoskeleton is crucial for the spontaneous formation of polarity. Note that here the cytoskeleton is not necessarily induced to polarize but is critically involved in generating the polarity itself.

Spontaneous cell polarity and directional persistence.

The earliest approach to unifying both persistence during non-directed motility and biased random walk during chemotaxis was based on the concept of fluctuations in receptor binding, or 'receptor noise' [79]. When the cell was in a uniform concentration of chemoattractant, small deviations from uniformity in localization or occupancy of the receptor were amplified by positive feedback leading to dynamical and morphological polarity required for persistence. Importantly, the magnitude of noise needed to reproduce adequate persistence was large enough to also explain the random aspects of chemotaxis. The simplicity of this notion provided a strong unifying hypothesis to explain the existence of directional persistence during non-directed motility and the biased random walk of cells during chemotaxis. In a sense, the model supposed polarity to be driven by instabilities. However, it is now clear that some cells can perform persistent random walks in the absence of any ligand, or for that matter, even

constitutive receptor activity. Thus the instability must come from some other source than the receptor.

Equally important are observations of the spontaneous activity or production of classic signaling molecules originally identified as regulators of chemotaxis. Although PI3K, PTEN, and Ras were originally shown to localize to the leading edge during chemotaxis, they have also been showed to localize to (or delocalize from, in the case of PTEN) sites of membrane protrusion during non-directed motility [57]. Importantly, the spontaneous translocation of these signaling molecules has been shown to occur in cells lacking the only Gβ subunit in *Dictyostelium*, thus revealing the translocation to be independent of classical receptor constitutive activity. Additionally, the spontaneous localization of PI3K required a fully function F-actin cytoskeleton as the spontaneous dynamics of PI3K were eliminated by treatment with the F-actin inhibitor Latrunculin. Similarly, the spontaneous activity of PI3K has also been observed in neutrophils and fibroblasts [98, 99]. These observations led to the postulation of feedback between the F-actin cytoskeleton and important signaling molecules.

Speculation on the pathways leading to spontaneous polarity.

The identity of the molecular components that are responsible for breaking symmetry and leading to spontaneous cell polarity in Dictyostelium are not known. Multiple pathways have been implicated in polarization and the formation of protrusions (see Chapter I). The presence of persistence, albeit relatively low, during vegetative non-directed motility suggests

that the most basic (and perhaps simplest) form of spontaneous cell polarity exists in this form of motility. It seems likely that in the vegetative state, the cellular concentrations of the key polarity components and the rate constants that govern their interaction are tuned to allow for a basic form of spontaneous polarity and directional persistence. It is here that we are likely to identify core mechanisms of spontaneous cell polarity. The other forms of motility, i.e., those with greater directional persistence, are then likely to result from the tweaking of this core system by either altering the concentrations or rate constants to further encourage spontaneous cell polarity and directional persistence (for example, during developed non-directed motility) or by the addition of new layers of regulation through receptor-driven or feedback –driven signal transduction (for example, chemotaxis or developed non-directed motility, respectively).

We suggest that, in its most basic form, the ability to spontaneously polarize lies within the F-actin/myosin cytoskeleton itself and perhaps a few key regulators that initiate F-actin regulation. In this scenario, fluctuations in key F-actin regulators, such as WASP, SCAR, or Formins initiate F-actin polymerization. Single knockouts of all three of these actin polymerization initiators show defects in chemotaxis and non-directed motility. In our study (Fig. 16) we show that loss of WASP function, but not SCAR function, leads to an quantitatively altered scaling relationship between persistence time and reorientation time. Future work will investigate the bimodal behavior in these cell lines in more detail, particularly during vegetative motility.

With the core mechanisms for spontaneous cell polarity and directional persistence in place, the cell would then be free to add multiple layers of regulation via signal transduction to these intrinsic, spontaneous processes. In particular, the PI3K pathway has been shown to be involved in polarization. Furthermore, it has been implicated in complex feedback from the F-

actin cytoskeleton during both vegetative and developed motility. Our studies on cells lacking two of the five type I PI3Ks failed to detect any significant differences compared to *wt*. Whether this is due to the remaining PI3K isoforms or t o PI3K-independent processes is not known. The fact that multiple pathways have been shown through genetics to be important, but not required for proper cell motility or chemotaxis, might imply that the basic ability of the cell to spontaneous polarize and regulate the polarity is due to multiple, redundant pathways.

An approach to isolate of core mechanisms of spontaneous polarity and directional persistence from additional layers of complexity that stabilize the polarity and increase persistence would be to compare $\overline{t}_p$ and $\overline{t}_r$ of mutants in vegetative and developed non-directed motility and chemotaxis. According to our hypothesis, we expect some mutants to have lower values of $\overline{t}_p$ compared to *wt* for all assays and some to only display altered persistence during developed non-directed motility or chemotaxis. Those mutants that are deficient in persistence in all assays would be classified as contributing to core mechanisms of spontaneous polarity while those that only display defects as developed cells would then be considered to belong to the additional regulatory layers.

An integrated approach to chemotaxis.

Spontaneous polarity versus chemoattractant-induced polarity.

The study of chemotaxis has focused on the regulation of the actin-myosin cytoskeleton by signal transduction (see [5] for an example). In this view, both

dynamical and morphological cell polarity is induced by signal transduction, as a result of asymmetric chemoattractant receptor occupancy. Implicit in such a view is that signaling plays an active, instructive role, while the cytoskeleton plays a more passive part. However, studies of spontaneous cell polarity have shown that cell polarity results from stochastic fluctuations in the dynamics of actin-cytoskeleton and its core regulatory proteins. Our results clearly demonstrate that cells can move with directional persistence in the absence of receptor-induced signaling.

Seen within the light of the results reviewed above, our data leads to the proposition that cell motility, including both directed and non-directed, results from a cycle of repeated spontaneous cell polarity. During non-directed motility, small fluctuations are amplified due to the unstable nature of the actin cytoskeleton and its core regulatory accessory molecules. These amplified fluctuations lead to cell polarity and directionally persistent motility. This cell polarity, consisting of the spontaneously orchestrated activity of numerous molecular processes distributed throughout the cell, is volatile and eventually dissipates, and the underlying processes of actin regulation become uncoordinated. This lack of sub-cellular coordination is revealed in the lack of directional persistence during reorientation mode.

During chemotaxis, concentration gradients harness this cyclic polarization-depolarization cycle to result in highly persistent, directed motility. We propose that chemoattractant gradients, in addition to orienting the direction of polarization, either stabilize the persistent mode, increase the frequency of the transition into persistent mode, or both, to result in motility that appears highly directed and persistent. The

tendency of a cell to move with persistence could have important effects in chemotaxis. As a result, the cell would be able to pause, determine direction by averaging over time, then move in that direction with persistence. Such a strategy would increase the accuracy of motility by relieving the cell of the need for constant, instantaneous measurements of the chemoattractant gradient.

Cell motility as repeated symmetry breaking.

Seen within the light of the results reviewed above, our data leads to the proposition that cell motility, including both directed and non-directed, results of a cycle of repeated symmetry breaking. During non-directed motility, small fluctuations are amplified to the unstable nature of the system consisting of the actin cytoskeleton and its core regulatory accessory molecules. These amplified fluctuations lead to cell polarity and directionally persistent motility. This cell polarity, consisting of the spontaneously orchestrated activity of numerous molecular processes distributed throughout the cell, is volatile and eventually dissipates, and the underlying processes of actin regulation become uncoordinated. This lack of sub-cellular coordination in revealed in the lack of directional persistence during reorientation mode.

During chemotaxis, concentration gradients harness this cyclic polarization-depolarization cycle to result in highly persistent, directed motility. We propose that chemoattractant gradients, in addition to orienting the direction of polarization, either stabilize the persistent mode, increase the frequency of the transition into persistent mode, or both, to result in motility that appears to be highly directed and purposeful.

Pseudopodia dynamics during non-directed motility and chemotaxis.

Very recent work by van Haastert and colleagues has focused on the dynamics of pseudopod extension during motility [100-102]. A central claim underlying their work is that pseudopod protrusion is the fundamental determinant of amoeboid cell motility. They obtain a very detailed description of pseudopodia extension, a description that appears to provide considerable insight into *Dictyostelium* motility.

After observing numerous *Dictyostelium* cells moving, Bosgraf and van Haastert claim that the spatial orientation of pseudopod production is far from random. In fact, nearly all pseudopodia produced during motility fall into one of two categories: 1) split pseudopodia, or those that form by splitting from existing pseudopodia, or 2) *de novo,* or those that are produced at apparently random positions around the cell cortex. The split pseudopodia, then, are that are strictly formed in close proximity to existing pseudopodia, while *de novo* pseudopodia are produced without relation to existing pseudopodia.

This classification is taken further by the argument that all motility, including directionally persistent and reorientation is the result of the dynamics of these two types of pseudopodia. Specifically, it is claimed that directionally persistent motion is the result of successive split pseudopodia while the interruption of directionally persistent motion is the result of *de novo* pseudopodia. The ratio of split to *de novo* pseudopodia, then, defines the amount of persistence in a cell's trajectory and

differential regulation of this ratio is responsible for the full range of *Dictyostelium* motility.

It is an exciting possibility that our measurements of directional persistence and reorientation might be related to the pseudopodia dynamics reported in [100-102]. A cursory examination of the data suggests that as cells transition from vegetative to developed, the do increase the ratio of split/*de novo* pseudopodia in a manner consistent with our scaling law. In such a scenario, the scaling law would be a high-order principle that governs the ratio of split/*de novo* pseudopodia. However, there are a few concerns regarding any attempt to explain our scaling law strictly in terms of pseudopod production.

First, the speculation about pseudopodia being the sole determinant of amoeboid motility is never directly examined by van Haastert and colleagues. For example, it is well know that the retraction of the uropod is also an important aspect of motility. Second, we succeeded in generalizing our scaling law to human cells including neutrophils, epithelial, and fibrosarcoma cells. It is well appreciated that cells such as epithelial cells and fibroblast move slowly, with a broad and relatively stable lamella, limiting application of the idea of split/*de novo* pseudopodia to all motile cells. However, a more general concept of dynamical cell polarity, where efficient, persistent motility is the result of organized, spatially restricted F-actin based protrusion complemented with retraction is generally applicable to all the cell lines in our study. In this scenario, the split pseudopodia of are the method used by *Dictyostelium*, with its high speed and

sometimes erratic motility, once the polarity has been established. Other cell lines, such as epithelial cells utilize a more stable lamella and move at a different time scale.

The next generation of models of gradient sensing.

All current models of gradient sensing assume that every movement initiated by the cell during chemotaxis is regulated by receptor-driven signal transduction. Although the stochastic nature if the chemoattractant-receptor interaction is fully appreciated, the mechanical activities of the cytoskeleton are treated as if they are passively controlled by a deterministic signal transduction network. By equine analogy, it is as if the cell is a blind and lazy mule that will not budge unless forced by a driver. According to the model presented here the cell, with its predilection for spontaneous polarization and directional persistence is more like a thoroughbred before a race, side-stepping and trotting in tight and tense anticipation. When the gates open, the rider simply controls how the pent-up energy is dissipated in the swift, directed movement. Future, more realistic models of gradient sensing must take in to account the ability of the cell to spontaneously polarize and move with directional persistence independent of chemoattractant signaling.

BIBLIOGRAPHY

1. Alberts, B., *Molecular Biology of the Cell in Cell 4th*, Figure.

2. Lodish, H.F., *Molecular cell biology*. 2003: WH Freeman.

3. Bray, D., *Cell movements*. 1992: Garland New York.

4. Yam, P.T., et al., *Actin-myosin network reorganization breaks symmetry at the cell rear to spontaneously initiate polarized cell motility.* J Cell Biol, 2007. **178**(7): p. 1207-21.

5. Affolter, M. and C.J. Weijer, *Signaling to cytoskeletal dynamics during chemotaxis.* Dev Cell, 2005. **9**(1): p. 19-34.

6. Kessin, R.H. and J. Franke, *Dictyostelium: evolution, cell biology, and the development of multicellularity*. 2001: Cambridge Univ Pr.

7. Eichinger, L., et al., *The genome of the social amoeba Dictyostelium discoideum.* Nature, 2005. **435**(7038): p. 43-57.

8. Thompson, D., A. Wentworth, and J.T. Bonner, *On growth and form*. 1992: Cambridge University Press Cambridge, UK.

9. Shields, J.M. and W.S. Haston, *Behaviour of neutrophil leucocytes in uniform concentrations of chemotactic factors: contraction waves, cell polarity and persistence.* J Cell Sci, 1985. **74**(1): p. 75-93.

10. Del Alamo, J.C., et al., *Spatio-temporal analysis of eukaryotic cell motility by improved force cytometry.* Proc Natl Acad Sci U S A, 2007. **104**(33): p. 13343-8.

11. Janetopoulos, C., et al., *Chemoattractant-induced phosphatidylinositol 3,4,5-trisphosphate accumulation is spatially amplified and adapts, independent of the actin cytoskeleton.* Proc Natl Acad Sci U S A, 2004. **101**(24): p. 8951-6.

12. Yumura, S., H. Mori, and Y. Fukui, *Localization of actin and myosin for the study of ameboid movement in Dictyostelium using improved immunofluorescence.* J Cell Biol, 1984. **99**(3): p. 894-9.

13. Samadani, A., J. Mettetal, and A. van Oudenaarden, *Cellular asymmetry and individuality in directional sensing.* Proceedings of the National Academy of Sciences, 2006. **103**(31): p. 11549.

14. Yoshida, K. and T. Soldati, *Dissection of amoeboid movement into two mechanically distinct modes.* J Cell Sci, 2006. **119**(Pt 18): p. 3833-44.

15. Song, L., et al., *Dictyostelium discoideum chemotaxis: threshold for directed motion.* Eur J Cell Biol, 2006. **85**(9-10): p. 981-9.

16. Xu, X., et al., *Quantitative imaging of single live cells reveals spatiotemporal dynamics of multistep signaling events of chemoattractant gradient sensing in Dictyostelium.* Molecular biology of the cell, 2005. **16**(2): p. 676-688.

17. Onsum, M.D., et al., *Morphology matters in immune cell chemotaxis: membrane asymmetry affects amplification.* Phys Biol, 2006. **3**: p. 190-199.

18. Kutscher, B., P. Devreotes, and P.A. Iglesias, *Local excitation, global inhibition mechanism for gradient sensing: an interactive applet.* Sci STKE, 2004. **2004**(219): p. pl3.

19. Franca-Koh, J. and P.N. Devreotes, *Moving forward: mechanisms of chemoattractant gradient sensing.* Physiology (Bethesda), 2004. **19**: p. 300-8.

20. Ueda, M., et al., *Single-molecule analysis of chemotactic signaling in Dictyostelium cells*. 2001. p. 864-867.

21. de Keijzer, S., et al., *A spatially restricted increase in receptor mobility is involved in directional sensing during Dictyostelium discoideum chemotaxis.* Journal of cell science, 2008. **121**(10): p. 1750.

22. Jin, T., et al., *Localization of the G protein betagamma complex in living cells during chemotaxis.* Science, 2000. **287**(5455): p. 1034-6.

23. Janetopoulos, C., T. Jin, and P. Devreotes, *Receptor-mediated activation of heterotrimeric G-proteins in living cells.* Science, 2001. **291**(5512): p. 2408-11.

24. Sasaki, A.T., et al., *Localized Ras signaling at the leading edge regulates PI3K, cell polarity, and directional cell movement.* J Cell Biol, 2004. **167**(3): p. 505-18.

25. Funamoto, S., et al., *Spatial and temporal regulation of 3-phosphoinositides by PI 3-kinase and PTEN mediates chemotaxis.* Cell, 2002. **109**(5): p. 611-623.

26. Takeda, K., et al., *Role of phosphatidylinositol 3-kinases in chemotaxis in Dictyostelium.* J Biol Chem, 2007. **282**(16): p. 11874-84.

27. Iijima, M. and P. Devreotes, *Tumor suppressor PTEN mediates sensing of chemoattractant gradients.* Cell, 2002. **109**(5): p. 599-610.

28. Leslie, N.R., et al., *PtdIns(3,4,5)P(3)-dependent and -independent roles for PTEN in the control of cell migration.* Curr Biol, 2007. **17**(2): p. 115-25.

29. Ferguson, G.J., et al., *PI (3) K? has an important context-dependent role in neutrophil chemokinesis.* Nature Cell Biology, 2006. **9**(1): p. 86-91.

30. Menager, C., et al., *PIP3 is involved in neuronal polarization and axon formation.* Journal of neurochemistry, 2004. **89**(1): p. 109.

31. Menager, C., et al., *PIP3 is involved in neuronal polarization and axon formation.* J Neurochem, 2004. **89**(1): p. 109-18.

32. Pinal, N., et al., *Regulated and polarized PtdIns(3,4,5)P3 accumulation is essential for apical membrane morphogenesis in photoreceptor epithelial cells.* Curr Biol, 2006. **16**(2): p. 140-9.

33. Martin-Belmonte, F., et al., *PTEN-mediated apical segregation of phosphoinositides controls epithelial morphogenesis through Cdc42.* Cell, 2007. **128**(2): p. 383-97.

34. Hoeller, O. and R.R. Kay, *Chemotaxis in the absence of PIP3 gradients.* Curr Biol, 2007. **17**(9): p. 813-7.

35. Chen, L., et al., *PLA2 and PI3K/PTEN pathways act in parallel to mediate chemotaxis.* Dev Cell, 2007. **12**(4): p. 603-14.

36. Kamimura, Y., et al., *PIP3-independent activation of TorC2 and PKB at the cell's leading edge mediates chemotaxis.* Curr Biol, 2008. **18**(14): p. 1034-43.

37. Fisher, P.R., R. Merkl, and G. Gerisch, *Quantitative analysis of cell motility and chemotaxis in Dictyostelium discoideum by using an image processing system and a novel chemotaxis chamber providing stationary chemical gradients.* Journal of Cell Biology, 1989. **108**(3): p. 973-984.

38. van Haastert, P.J. and M. Postma, *Biased random walk by stochastic fluctuations of chemoattractant-receptor interactions at the lower limit of detection.* Biophys J, 2007. **93**(5): p. 1787-96.

39. Chen, M.Y., R.H. Insall, and P.N. Devreotes, *Signaling through chemoattractant receptors in Dictyostelium.* Trends in Genetics, 1996. **12**(2): p. 52-57.

40. Ueda, M. and T. Shibata, *Stochastic signal processing and transduction in chemotactic response of eukaryotic cells.* Biophys J, 2007. **93**(1): p. 11-20.

41. Urbach, J.S. and G.J. Goodhill, *Limitations on detection of gradients of diffusible chemicals by axons.* Neurocomputing, 1999. **26**(1): p. 39-44.

42. Endres, R.G. and N.S. Wingreen, *Accuracy of direct gradient sensing by single cells.* Proceedings of the National Academy of Sciences, 2008. **105**(41): p. 15749.

43. van Haastert, P.J., I. Keizer-Gunnink, and A. Kortholt, *Essential role of PI3-kinase and phospholipase A2 in Dictyostelium discoideum chemotaxis.* J Cell Biol, 2007. **177**(5): p. 809-16.

44. Jeon, T.J., et al., *Regulation of Rap1 activity by RapGAP1 controls cell adhesion at the front of chemotaxing cells.* J Cell Biol, 2007. **179**(5): p. 833-43.

45. Funamoto, S., et al., *Spatial and temporal regulation of 3-phosphoinositides by PI 3-kinase and PTEN mediates chemotaxis.* Cell, 2002. **109**(5): p. 611-23.

46. J. G. Sai, G.M.W., J. P. Wikswo, and A. Richmond, *a P13K-independent, src-dependent, signal transduction pathway leads to rac2 activation and chemotaxis. .* Submitted, 2007.

47. Liu, Y., et al., *Microfluidic switching system for analyzing chemotaxis responses of wortmannin-inhibited HL-60 cells.* Biomed Microdevices, 2008.

48. Haugh, J.M., et al., *Spatial sensing in fibroblasts mediated by 3' phosphoinositides.* J Cell Biol, 2000. **151**(6): p. 1269-80.

49. Wang, F., et al., *Lipid products of PI(3)Ks maintain persistent cell polarity and directed motility in neutrophils.* Nat Cell Biol, 2002. **4**(7): p. 513-8.

50. Miyanaga, Y., et al., *Stochastic signal inputs for chemotactic response in Dictyostelium cells revealed by single molecule imaging techniques.* Biosystems, 2007. **88**(3): p. 251-60.

51. Xu, X., et al., *Quantitative imaging of single live cells reveals spatiotemporal dynamics of multistep signaling events of chemoattractant gradient sensing in Dictyostelium.* Mol Biol Cell, 2005. **16**(2): p. 676-88.

52. Postma, M., et al., *Uniform cAMP stimulation of Dictyostelium cells induces localized patches of signal transduction and pseudopodia.* Mol Biol Cell, 2003. **14**(12): p. 5019-27.

53. Samadani, A., J. Mettetal, and A. van Oudenaarden, *Cellular asymmetry and individuality in directional sensing.* Proc Natl Acad Sci U S A, 2006. **103**(31): p. 11549-54.

54. Devreotes, P. and C. Janetopoulos, *Eukaryotic chemotaxis: distinctions between directional sensing and polarization.* J Biol Chem, 2003. **278**(23): p. 20445-8.

55. Andrew, N. and R.H. Insall, *Chemotaxis in shallow gradients is mediated independently of PtdIns 3-kinase by biased choices between random protrusions.* Nat Cell Biol, 2007. **9**(2): p. 193-200.

56. Wessels, D., et al., *PTEN plays a role in the suppression of lateral pseudopod formation during Dictyostelium motility and chemotaxis.* J Cell Sci, 2007. **120**(Pt 15): p. 2517-31.

57. Sasaki, A.T., et al., *G protein-independent Ras/PI3K/F-actin circuit regulates basic cell motility.* J Cell Biol, 2007. **178**(2): p. 185-91.

58. Whitesides, G.M., et al., *Soft lithography in biology and biochemistry.* Annu Rev Biomed Eng, 2001. **3**: p. 335-73.

59. Shim, J., et al., *Micro- and nanotechnologies for studying cellular function.* Curr Top Med Chem, 2003. **3**(6): p. 687-703.

60. Walker, G.M., et al., *Effects of flow and diffusion on chemotaxis studies in a microfabricated gradient generator.* Lab Chip, 2005. **5**(6): p. 611-8.

61. Glantz, S.A.a.S., B.K., *Primer of Applied Regression and Analysis of Variance*. 2 ed. 2001, New York: McGraw-Hill. 949.

62. Van Haastert, P.J. and M. Postma, *Biased Random Walk by Stochastic Fluctuations of Chemoattractant-Receptor Interactions at the Lower Limit of Detection.* Biophys J, 2007.

63. Crank, J., *The Mathematics of Diffusion*. 2nd ed. 1975, London: Oxford University Press. 414.

64. Fache, S., et al., *Calcium mobilization stimulates Dictyostelium discoideum shear-flow-induced cell motility.* J Cell Sci, 2005. **118**(Pt 15): p. 3445-57.

65. Decave, E., et al., *Shear flow-induced motility of Dictyostelium discoideum cells on solid substrate.* J Cell Sci, 2003. **116**(Pt 21): p. 4331-43.

66. Loovers, H.M., et al., *Distinct roles of PI(3,4,5)P3 during chemoattractant signaling in Dictyostelium: a quantitative in vivo analysis by inhibition of PI3-kinase.* Mol Biol Cell, 2006. **17**(4): p. 1503-13.

67. Arrieumerlou, C. and T. Meyer, *A local coupling model and compass parameter for eukaryotic chemotaxis.* Dev Cell, 2005. **8**(2): p. 215-27.

68. Vicker, M.G., *The regulation of chemotaxis and chemokinesis in Dictyostelium amoebae by temporal signals and spatial gradients of cyclic AMP.* J Cell Sci, 1994. **107 (Pt 2)**: p. 659-67.

69. Campbell, K. and A. Groisman, *Generation of complex concentration profiles in microchannels in a logarithmically small number of steps.* Lab Chip, 2007. **7**(2): p. 264-72.

70. Andrews, B.W. and P.A. Iglesias, *An information-theoretic characterization of the optimal gradient sensing response of cells.* PLoS Comput Biol, 2007. **3**(8): p. e153.

71. Li, L., S.F. Norrelykke, and E.C. Cox, *Persistent cell motion in the absence of external signals: a search strategy for eukaryotic cells.* PLoS ONE, 2008. **3**(5): p. e2093.

72. Selmeczi, D., et al., *Cell motility as persistent random motion: theories from experiments.* Biophys J, 2005. **89**(2): p. 912-31.

73. Potdar, A.A., et al., *Bimodal analysis of mammary epithelial cell migration in two dimensions.* Ann Biomed Eng, 2009. **37**(1): p. 230-45.

74. Gruver, J.S., J.P. Wikswo, and C.Y. Chung, *3'-phosphoinositides regulate the coordination of speed and accuracy during chemotaxis.* Biophys J, 2008. **95**(8): p. 4057-67.

75. Saltzman, W.M., *Tissue Engineering : Engineering Principles for the Design of Replacement Organs and Tissues*. 2004, New York: Oxford University Press.

76. Doi, M. and S.F. Edwards, *The theory of polymer dynamics*. 1986, New York: Oxford Univeristy Press.

77. Uhlenbeck, G.E. and L.S. Ornstein, *On the theory of the Brownian motion.* Physical Review, 1930. **36**: p. 823-841.

78. Bretschneider, T., et al., *Dynamic actin patterns and Arp2/3 assembly at the substrate-attached surface of motile cells.* Curr Biol, 2004. **14**(1): p. 1-10.

79. Tranquillo, R.T., D.A. Lauffenburger, and S.H. Zigmond, *A stochastic model for leukocyte random motility and chemotaxis based on receptor binding fluctuations.* J Cell Biol, 1988. **106**(2): p. 303-9.

80. Bak, P., C. Tang, and K. Wiesenfeld, *Self-organized criticality.* Phys Rev A, 1988. **38**(1): p. 364-374.

81. Benichou, O., et al., *Optimal search strategies for hidden targets.* Phys Rev Lett, 2005. **94**(19): p. 198101.

82. Maeda, Y.T., et al., *Ordered patterns of cell shape and orientational correlation during spontaneous cell migration.* PLoS ONE, 2008. **3**(11): p. e3734.

83. Etienne-Manneville, S. and A. Hall, *Cdc42 regulates GSK-3beta and adenomatous polyposis coli to control cell polarity.* Nature, 2003. **421**(6924): p. 753-6.

84. Stites, J., et al., *Phosphorylation of the Dictyostelium myosin II heavy chain is necessary for maintaining cellular polarity and suppressing turning during chemotaxis.* Cell Motil Cytoskeleton, 1998. **39**(1): p. 31-51.

85. Myers, S.A., et al., *A Dictyostelium homologue of WASP is required for polarized F-actin assembly during chemotaxis.* Mol Biol Cell, 2005. **16**(5): p. 2191-206.

86. Shenderov, A.D. and M.P. Sheetz, *Inversely correlated cycles in speed and turning in an ameba: an oscillatory model of cell locomotion.* Biophys J, 1997. **72**(5): p. 2382-9.

87. Fabry, B., et al., *Scaling the microrheology of living cells.* Phys Rev Lett, 2001. **87**(14): p. 148102.

88. Stamenovic, D., et al., *Rheological behavior of living cells is timescale-dependent.* Biophys J, 2007. **93**(8): p. L39-41.

89. Kozubowski, L., et al., *Symmetry-breaking polarization driven by a Cdc42p GEF-PAK complex.* Curr Biol, 2008. **18**(22): p. 1719-26.

90. Ozbudak, E.M., A. Becskei, and A. van Oudenaarden, *A system of counteracting feedback loops regulates Cdc42p activity during spontaneous cell polarization.* Dev Cell, 2005. **9**(4): p. 565-71.

91. Dobereiner, H.G., et al., *Lateral membrane waves constitute a universal dynamic pattern of motile cells.* Phys Rev Lett, 2006. **97**(3): p. 038102.

92. Gerisch, G., et al., *Mobile actin clusters and traveling waves in cells recovering from actin depolymerization.* Biophys J, 2004. **87**(5): p. 3493-503.

93. Weiner, O.D., et al., *An actin-based wave generator organizes cell motility.* PLoS Biol, 2007. **5**(9): p. e221.

94. Gerhart, J. and M. Kirschner, *Cells, embryos, and evolution: Toward a cellular and developmental understanding of phenotypic variation and evolutionary adaptability*. 1997: Blackwell Science Malden, MA.

95. Wedlich-Soldner, R., et al., *Spontaneous cell polarization through actomyosin-based delivery of the Cdc42 GTPase*. 2003. p. 1231-1235.

96. Xu, J., et al., *Divergent signals and cytoskeletal assemblies regulate self-organizing polarity in neutrophils.* Cell, 2003. **114**(2): p. 201-214.

97. Weiner, O.D., et al., *A PtdInsP(3)- and Rho GTPase-mediated positive feedback loop regulates neutrophil polarity.* Nat Cell Biol, 2002. **4**(7): p. 509-13.

98. Inoue, T. and T. Meyer, *Synthetic activation of endogenous PI3K and Rac identifies an AND-gate switch for cell polarization and migration.* PLoS ONE, 2008. **3**(8): p. e3068.

99. Weiger, M.C., et al., *Spontaneous phosphoinositide 3-kinase signaling dynamics drive spreading and random migration of fibroblasts.* J Cell Sci, 2009. **122**(Pt 3): p. 313-23.

100. Bosgraaf, L. and P.J. Van Haastert, *Navigation of chemotactic cells by parallel signaling to pseudopod persistence and orientation.* PLoS One, 2009. **4**(8): p. e6842.

101. Bosgraaf, L. and P.J. Van Haastert, *The ordered extension of pseudopodia by amoeboid cells in the absence of external cues.* PLoS One, 2009. **4**(4): p. e5253.

102. Van Haastert, P.J. and L. Bosgraaf, *Food searching strategy of amoeboid cells by starvation induced run length extension.* PLoS One, 2009. **4**(8): p. e6814.